

**Stability of Silver Colloid by Process Control of the Synthesis using
Design of Experiments**

by

YARENI PATRICIA LARA RODRÍGUEZ

A thesis submitted in partial fulfillment of the requirements for the degree of

MASTER OF SCIENCE

in

**MECHANICAL ENGINEERING
UNIVERSITY OF PUERTO RICO
MAYAGÜEZ CAMPUS
2013**

Approved by:

Ricky Valentín, Ph.D.
Member, Graduate Committee

Date

Mauricio Cabrera, Ph.D.
Member, Graduate Committee

Date

Pedro Quintero, Ph.D.
President, Graduate Committee

Date

Jaime Ramirez Vick, Ph.D.
Representative of Graduate Studies

Date

Ricky Valentín, Ph.D.
Chairperson of the Department

Date

ABSTRACT

Extensive resources have been utilized to develop SiC (silicon carbide) semiconductor devices, there has been relatively little effort into the development of adequate, environmentally benign electronic packaging materials and methods to provide functional modules that will enable and take full advantage of the capabilities of these SiC devices. A critical requirement for any metallic interconnection within an electronic package is that the joint cannot re-melt during the operation. This condition implies a rule in which the attach material has to be selected as such, that its melting temperature (T_m) must be higher than the application temperature (T_a). Therefore a novel alternative will have to result in a high melting attach material that can be processed at a low enough temperature to avoid excessive residual stresses.

An alternative, and possible solution is the use Ag nanoparticles, these particles can be used as an attach material owing to its excellent thermal and electrical properties in addition to its high melting point (962°C). Theoretically the driving force (DF) for the sintering mechanism is a function of the applied pressure (P) and a geometrical factor (K) which is inversely proportional to the particle size ($K \propto 1/s$). Increasing the densification rate is crucial in a sintering process, therefore to achieve this densification it is desired to apply a low pressure for the minimum possible time. Thus, to provide a large driving force, without increasing the detrimental externally applied pressure, we proposed to take advantage of the size effect of Ag nanoparticles.

In this work a methodology for the manufacture of stable silver nanoparticles (NP's) was proposed together with a prediction model for these parameters. To reach the aims of this work, Ag nanoparticles were produced by chemical reduction method. During the preparation, reducing agent directly reduced Ag^+ ions to generate metallic Ag atoms and the borohydride from $NaBH_4$ (reducer agent) were absorbed on the surface of the Ag atoms giving a electrostatic mechanism effect in order to avoid early agglomeration.

A factorial design of experiments 2^3 with three replicates (24 runs) plus a center point with three replicates (27 trials in total) were proposed with the objective to explore the feasible area of elaboration of nanoparticles with stability. The factors were the concentration rate $[R=\text{NaBH}_4/\text{AgNO}_3]$ (1, 12.5 and 26), stirrer time (50% , 100% and 150%) and temperature (0°C, 7.5 °C and 15°C). The synthesis was elaborated with DI water 17M Ω at room temperature.

The size and *size slope* of the NP's was characterized via X-ray diffraction (XRD), UV-Vis and DLS. The results showed that was possible to find stabilization in a feasible area of synthesis when the concentration rate (R) was 12.5 and the stirrer time was 100%, in addition, low level of temperature also helped to reach the stabilization of NP's. The statistical model for the prediction of size and slope of was obtained.

RESUMEN

Amplios recursos se han utilizado para desarrollar dispositivos semiconductores de SiC (carburo de silicio), y ha habido relativamente poco esfuerzo en el desarrollo de materiales de empaquetamiento electrónico adecuados y ambientalmente benignos y métodos para proporcionar módulos funcionales que permitan aprovechar al máximo las capacidades de estos dispositivos de SiC. Un requisito esencial para cualquier interconexión metálica dentro de un empaquetamiento electrónico es que la unión inter metálica no pueda volverse a fundir durante la operación. Esta condición implica una regla en la que el material para la soldadura tiene que ser seleccionado como tal, que su temperatura de fusión (T_m) debe ser superior a la temperatura de aplicación (T_a). Por lo tanto una alternativa novedosa tendrá que dar lugar a un alto punto de fusión del material para soldar y que se pueda procesar a una temperatura suficientemente baja para evitar un exceso de estrés residual.

Una alternativa, y posible solución es el uso de nanopartículas de plata, estas partículas se pueden utilizar como un material de soldadura debido a sus excelentes propiedades térmicas y eléctricas, además de su alto punto de fusión (962°C). Teóricamente la fuerza motriz (DF) para el mecanismo de sinterización es una función de la presión aplicada (P) y un factor geométrico (K) que es inversamente proporcional al tamaño de partícula ($K \propto 1 / s$). El aumento de la tasa de densificación es crucial en un proceso de sinterización, por lo tanto, para lograr esta densificación se desea aplicar una presión baja para el mínimo tiempo posible. Por lo tanto, para proporcionar una fuerza de accionamiento grande, sin aumentar la perjudicial presión aplicada externamente, se propone aprovechar el efecto del tamaño de nanopartículas de Ag.

En este trabajo se propone una metodología para la fabricación de nanopartículas de plata estables en solución acuosa junto con un modelo de predicción para estos parámetros. Para alcanzar los objetivos de este trabajo, las nanopartículas de Ag fueron producidas por el método de reducción química. Durante la preparación, el agente reductor reduce directamente los iones Ag^+ para generar átomos metálicos de Ag y el borohidruro proveniente de NaBH_4 (agente reductor) se ha absorbido en la superficie de los átomos de Ag dando un mecanismo de efecto electrostático con el fin de evitar la aglomeración.

Un diseño factorial de experimentos 2^3 con tres réplicas (24 corridas) más un punto centro con tres réplicas (3 corridas más 27, corridas en total) se han propuesto con el objetivo de explorar el área factible de elaboración de las nanopartículas con la mayor estabilidad. Los factores fueron la tasa de concentración de $[\text{R} = \text{NaBH}_4/\text{AgNO}_3]$ (1 a 26), el tiempo de agitación (50% a 150%) y la temperatura (0°C a 15°C). La síntesis fue elaborada con agua de-ionizada de $17\text{M}\Omega$ a temperatura ambiente.

El tamaño y la pendiente de la partícula se caracterizó mediante difracción de rayos X (XRD), UV-Vis y DLS. Los resultados mostraron que era posible encontrar una zona factible de estabilización en la síntesis cuando la tasa de concentración (R) fue de 12,5 y el tiempo de agitación fue de 100%, además, bajo nivel de temperatura también ayudó a alcanzar la estabilización de los NP's. Se logro obtener el modelo estadístico para la predicción de tamaño de partícula y su cambio en el tiempo.

Copyright© by

Yareni P Lara-Rodríguez

2013

All rights reserved. Printed in the United States of America. Except as permitted under the United States Copyright Act of 1976, no part of this publication may be reproduced or distributed in any form or by any means, or stored in a data base or retrieved system, without the prior written permission of the publisher.

Dedicated to

My precious parents

Francisco Lara ⁽⁺⁾ and Silvia Rodríguez

and to my wonderful sisters

Silvia, Socorro, María and Hilda

With all my love

ACKNOWLEDGMENTS

First of all I want to thank God for being my guidance in this stage of my life.

I would like to thank my advisor Professor Pedro O Quintero Aguilo for giving to me the opportunity to work with him, for his friendship, motivation, patience and for all the imparted knowledge.

To National Science Foundation (NSF), for the partial fellowship during my Master Studies

To Professor Mauricio Cabrera-Ríos for his friendship, motivation in this important stage of my life and for his help with my thesis work.

To Professor Ricky Valentin for the revision of this work.

I would especially like to thank:

The personal of Mechanical Engineering Department at UPRM

Boris Rentería and Professor Oscar Perales for the XRD, UV-Vis and DLS measurements.

Andrés Velasco, Alfredo Díaz, Ana Lucía Vega, Manuel Molina and Rogie Rodríguez for all their help, friendship and for the knowledge provided.

Joel Rodriguez from Center writing for the English revision of my thesis.

Table of Content

1	INTRODUCTION	12
1.1	Hypothesis of this work.....	14
1.2	Motivation.....	14
	Objetives.....	15
2	PREVIOUS RELATED WORK.....	16
2.1	Introduction: importance and methods of Ag NP's fabrication.....	16
2.2	Selection of parameters for stability in Ag colloid systems	19
3	THEORETICAL BACKGROUND	20
3.1	Preview.....	20
3.2	Nucleation and growth of NP's	20
3.3	Oxidation-Reduction Method (Redox)	21
3.4	Stability in colloids Ag NP's	22
3.5	Derjaguin, Landau, Verwey and Overbeek theory(DLVO theory).	22
3.6	Mechanism of formation for silver nanoparticles by redox method.....	24
3.7	The Experimental Design.....	26
3.8	Design of experimental process.....	27
3.9	The 2 ³ Design.....	29
3.10	P value and Determining Sample Size	33
4	MATERIAL CHARACTERIZATION TECHNIQUES	35
4.1	Preview.....	35
4.2	The Z-Sizer NanoS90 Instrument.....	35
4.3	Dynamic light scattering (DLS).....	36
4.4	Zeta potential	37

4.5	X-ray Diffraction	38
4.6	Ultraviolet/Visible Spectroscopy (UV-vis)	40
4.7	UV/Visible spectra	41
4.8	Plasmon in Ag NP's.....	42
5	EXPERIMENTAL PLANNING AND EXECUTION.....	44
5.1	Experimental Planning	44
5.2	Experimental execution.....	46
6	RESULTS AND DISCUSSION	50
6.1	Introduction.....	50
6.2	Interval plots analysis.....	51
6.2.1	Interval plot for the average size 1, size 2 and Z potential slope.....	52
6.2.2	Interval plots results for z potential slope values	55
6.2.3	Discussion for the interval plots.....	56
6.3	Colloid color analysis (Qualitative analysis)	58
6.4	Ultraviolet-visible (UV-vis) spectroscopy analysis (Qualitative analysis)	61
	X Ray Diffraction Analysis.....	63
6.5	Statistical Analysis (ANOVA).....	64
6.5.1	The p value for the average sizes and slope.....	64
6.5.2	Statistical model	67
6.5.3	Center points.....	81
6.6	Results from the combinations from design of experiments.....	82
6.7	Discussion of the effect for the concentration rate, temperature and stirrer time on the stability of Ag colloid	83
6.8	The best synthesis condition (combination)	84
7	Conclusions.....	85
8	REFERENCES	86

9	APPENDIX B	90
10	APPENDIX C	91
11	APPENDIX D	99
12	APPENDIX E.....	106

1 INTRODUCTION

Silicon carbide has become a very attractive material for high temperature and high power electronics applications due to its properties, which are different than those of conventional Si semiconductors. However, the reliability of SiC devices is limited by assembly processes such as die attachment and interconnections at high temperatures[1]. Within the electronic packaging process, it is at the first level interconnection where the die attachment to a substrate is achieved. For high-power applications, the die is usually eutectically bonded onto the package, using solder pastes of Au or Ag for good heat conduction. The die attachment compound should provide a good electrical and thermal path for the electronic interconnection [2][3]. A critical requirement for any metallic interconnection within an electronic package is that the joint cannot re-melt during the operation. This condition implies a rule in which the attach material has to be selected such that its melting temperature (T_m) must be higher than the application temperature (T_a). Therefore, a novel alternative will have to result in a high melting attach material that can be processed at a low enough temperature to avoid excessive residual stresses. However, the higher T_m requires the higher reflow temperature in the electronics manufacturing process, which has adverse effects not only on energy consumption but also on the package reliability, such as substrate warpage and thermal stresses. The melting point can be dramatically decreased when the size of the substances is reduced to nanometer size. To date, the size-dependent melting behavior has been found both theoretically and experimentally. The high surface area-to-volume ratio of nanoparticles has been known as one of the driving forces for the size dependent melting point depression, i.e., the reduction of metal nanoparticle melting point at small sizes [4] [5]. An alternative, and possible solution, is the sintering of Ag nanoparticles. These particles can be used as an attach material due to its excellent thermal and electrical properties in addition to its high melting point (962°C) [6] [7]. Sintering is a method used to fabricate objects from powders. It is based on atomic diffusion which occurs much faster at higher temperatures. Theoretically, the driving force (DF) for the sintering mechanism is a function of

the applied pressure (P) and a geometrical factor (K) which is inversely proportional to the particle size (s) ($K \propto 1/s$). Increasing the densification rate is crucial in a sintering process, therefore to achieve this densification it is desired to apply a low pressure for the minimum possible time, hence small particles are crucial for this process. A method for the fabrication of nanoparticles is chemical synthesis [8], among which the most common synthesis for silver nanoparticles is the reduction of a silver salt solution by a reducing agent such as NaBH_4 (sodium borohydride) and AgNO_3 (silver nitrate) as salt precursor. The use of a strong reducer, such as borohydride, tend to produce a narrow size distribution. It is also known that size control can be achieved by controlling the concentration of borohydride [9]. The chemical synthesis can be seen as a colloid system, which can be called “sol” when a solid is suspended in a liquid medium. The dispersed-phase particles have a diameter between approximately 1 and 1000 nanometers [10]. The system of Ag nanoparticles suspended in DI water can be represented as a colloid system and these Ag nanoparticles can be stabilized by two fundamental mechanisms: steric and electrostatic effects. The steric effect consists of using a capping agent over the nanoparticle to get the stable state of the nanoparticles, usually this capping agent can be a polymer which has been found to be a barrier to the required particle coagulation during sintering. The electrostatic effect consists of taking advantage of the attractive and repulsive forces between the positive surface charge of the nanoparticle and the anion in the colloid system. The steric repulsion involves polymers added to the system adsorbed onto the particle surface thus preventing the particle surfaces coming into close contact. The electrostatic, or charge stabilization, has the benefits of stabilizing or flocculating by altering the concentration of ions in the system. This is a reversible process and is potentially inexpensive [11]. The particles in a liquid move around randomly and their velocity of movement is used to determine the size of the particle. It is known that small particles move faster in a liquid and large particles move slower. By taking two “pictures” of the sample, separated by a short interval of time, the size of the particles can be inferred. If there has been minimal movement, and the particles position are very similar, then the particles in the sample are considered to be large; similarly if there has been a large amount of movement, and the particle positions are quite different, then the particles in the sample are considered small[12]. The nanoparticles size can be characterized by

measuring the Brownian motion of the particles in a sample using Dynamic Light Scattering (DLS), and then interpreting a size from this measurement using established theories [12].

A statistical tool, the ANOVA (Analysis of Variance) was used, from which an empirical model can be obtained with the objective to characterize the chemical process and to find which factors are significant in this process. This statistical model can be considered as starting point for optimizing the process [13].

The following section describes the hypothesis of this work.

1.1 Hypothesis of this work

The control of process parameters during the synthesis of Ag nanoparticles (NP's) can enable the stabilization of a colloid without the need of capping agents or surfactants.

1.2 Motivation

Studying the synthesis of silver nanoparticles for sintering applications will advance the realization of next generation power electronics, particularly for applications related to alternative energy and power. Pressureless sintering of Ag nanoparticles will enable a low temperature assembly operation that will yield a high temperature resistant interconnect, however the lack of stability of metallic nanopowders limits their application as an attach material. Therefore, controlling the stability during the synthesis is crucial in order to avoid early agglomerates, but it is also imperative to allow coagulation during sintering. Capping agents have proven to be excellent for controlling the coagulation, but they become a hurdle for sintering. In this work we are focus on controlling the synthesis process in such a way that temporary stabilization can occur but that the sintering is not affected when the processing comes into play.

Objetives

The principal objective of this work is to get stability in the Ag colloids and characterize the size of these nanoparticles, aimed at using these particles in pastes for the die attachment step of the electronic packaging process.

The specific research objectives of this work are:

- ✓ To develop a synthesis method for obtaining stable Ag NP's without surfactant
- ✓ To characterize the colloid Ag via X-ray diffraction (XRD), UV-Vis, and DLS.
- ✓ To apply a design of experiments as a tool in the synthesis process; to obtain empirical models as a function of critical parameters to stabilize the size of Ag nanoparticles.

The following chapter shows the previous work in the synthesis of Ag nanoparticles, stability, and applications of Ag nanoparticles.

2 PREVIOUS RELATED WORK

In this chapter, the previous related works for this thesis are presented in order to describe contributions which will help to achieve the aims. The contributions are presented in the following order: first, the common methods used for fabrication of Ag nanoparticles (NP's) and in second place the selection of parameters for stability in Ag colloids.

2.1 Introduction: importance and methods of Ag NP's fabrication

Nanotechnology deals with processes that take place at the nanometer scale, from approximately 1 to 100 nm. The properties of metal nanoparticles are different from those of bulk materials [14]. Several works report the importance of fabrication of NP's such as those of silver and gold due its electronic properties [15] [16]. The research on metal NP's has increased extensively in recent years due to their size dependent optical and chemical properties, also, the development of physical methods for their fabrication have enable large scale production together with correlations between optimal properties and their structure [17]. Specifically, silver nanoparticles have received extensive attention due to their potential in electronics applications.. As mentioned before, silver nanoparticles having fine or ultrafine sizes have attracted scientific interest because of their unusual properties compared to the bulk metal. Colloidal silver nano-particles, owing to their quantum size effects and surface effects, reveal excellent electrical conductivity and chemical stability. These properties have led to a tremendous range of applications of silver as die attach pastes in electronic packaging processes [18]. Another characteristic of silver colloids is that they show different colors due to light absorption and scattering in the visible spectral region. Plasmon resonance, the frequency at which conduction electrons oscillate in response to the alternating electric field of incident electromagnetic radiation, explain this behavior where the color of metal nanoparticles depends on the shape and the dielectric constant of the surrounding medium[19]. There are many methods to fabricate silver nanoparticles, these include template synthesis, silver mirror reaction,

polyol process, sol-gel process reverse micelle, photochemical or radiation chemical reduction, chemical vapor deposition, sonochemical synthesis, electrophoresis and electrochemical routes[20], with many studies attempting to correlate the particle size and morphology of silver sols to the reaction environment. However, the mechanism of growth and the origin of uniformity achieved in the reaction pathways are still largely unknown. The model typically used to explain the mechanism for the production of monodisperse colloidal particles is that of LaMer and Dinegar which argues that the number of particles in a solution is fixed in a very short burst of nucleation. Then particles grow by the addition of monomers (atomic species) at the surface of the new nuclei. Finally, continuous nucleation followed by aggregation may result in monodisperse particle size distributions[21]. Aggregation can be inhibited by the thick electrical double layers that form around metal nanoparticles in low-ionic-strength suspensions [22] [3].

The role of formation, size, and shape of advanced silver nanomaterials can be either accelerated or changed depending on the chemical system, nature of stabilizers, and the nature of the surfactant[23]. Zaheer Khana et al. showed how to obtain truncated triangular Ag particles using glucose and ammonia where the lowest concentrations of ammonia resulted in the smallest average size of and an intense maximum of the surface plasmon absorbance near of 420 nm. It is known that the absorption spectrum of silver nanoparticles is sharp and strong, a feature which is ascribed to the excitation of collective electron oscillations (so called surface plasmons) in response to an electromagnetic field [24].

Compared with the bulk material, silver (Ag) nanoparticles exhibit unique thermal and electrical properties due to their small-size and surface effect. Therefore, they have attracted great research interest and have been widely applied in the fields of electronics and microelectronics. In these fields, the silver nanoparticles are mainly used as the conductive functional phase to formulate electronic nanopastes. The nanopastes have some advantages over conventional micropastes. For example, they can save the content of precious metal, miniaturize the feature size of the electronic devices, decrease the temperature of heat treatment, and realize low-temperature sintering (the melting point of bulk silver metal is 960.3 °C, whereas the silver nanoparticles with 5–10nm diameter can be melted at only 150 °C)[25]. Particularly,

they are suitable for fabrication of flexible electronic devices, and have a potential to replace the conventional Sn–Pb solders in printed circuit board (PCB), integrated circuit (IC) and chip packaging for environmental reasons. The preparation of Ag nanoparticles also involves methods such as vacuum evaporation, electrical arc discharge, microemulsion, phase transfer, and chemical reduction-protection. Among them, chemical reduction-protection (redox) method is preferable because it has many merits (mild reaction condition, high yield, low energy consumption, and simple separating procedure) [25]. The chemical reduction method is the most used process for the synthesis of homogeneous and nano-sized metallic powders with low cost, fast, and mild solution conditions [8]. During the preparation, the surfactant in the reaction system plays a crucial role where it also acts as adsorbant and dispersant. And sometimes, surfactants or capping-agents, can be used to obtain desired shapes [26]. Many polymers and compounds, such as polyvinylpyrrolidone (PVP), alkanethiolate, alkaneamine, sodium dodecyl sulfate and sodium linoleate, have been sampled as surfactants. There are different reducing agents, J. Liu et al. for example, showed a method to synthesize silver nanoparticles by microemulsion using sodium borohydride (NaBH_4) and silver nitrate (AgNO_3). They found that the molar ratio of the reducing agent to silver nitrate is important. They observed that at a molar ratio higher than one, the obtained particles were of bigger size. In Martelli et al. it is mentioned that the NaBH_4 has a high potential to be used as reducing agent in industrial and laboratory applications due to its large volumetric and gravimetric hydrogen content. Borohydride anions are known to stabilize silver colloids through absorption on the particles. It is widely accepted that absorption colloids occur by an ensemble of electrostatic and weak interactions[27]. In the chemical reduction of silver ions a common reducing agent is sodium borohydride (NaBH_4) when nanosized silver colloids are wanted. Sodium borohydride is capable of reducing many metal ions because of its strong reducing power. In the case of silver, the reducing reaction is very intense, and a protective dispersing agent would not have sufficient time to coat each particle, so that the resulting particle sizes would increase as a result of agglomeration effects[28].

2.2 Selection of parameters for stability in Ag colloid systems

Sometimes it is possible to take control of a process from previous experience, but often the process response defies these predictions. In these cases, factorial experimentation (tool of design of experiments) can be the key to understanding the impact of each process input on the process outputs. Design of experiments technique provides a mathematical model that quantifies the effect of each input, allowing to determine the input settings to adjust the process so that the desired target is obtained [29] [30]. From previous works, it is suggested that for the synthesis of stable silver nanoparticles the critical factors of the synthesis are the temperature, concentration rate (NaBH_4)/[AgNO_3] [31] and stirrer time[14]. The levels proposed in these works are: from 0 to 15 °C for temperature, from 1 to 26 for concentration rate (NaBH_4)/[AgNO_3], and from 50 to 150% of the synthesis time for stirrer time factor . These parameters, and their levels were selected to control the size and stability of the Ag colloid system.

3 THEORETICAL BACKGROUND

3.1 Preview

This chapter describes the nucleation and growth process of nanoparticles, redox method (reduction-oxidation), stabilization of the colloid Ag NP's, the responses of interest, and the statistical tools used as part for the analysis of responses.

3.2 Nucleation and growth of NP's

The process parameters for the formation of nanoparticles are particularly important for the control of particle size and aggregation as well as composition for the case of more complex particles[2][32]. The particle size and aggregation effect depends on the nucleation rate and growth. As it was seen in previous related work section, the stirrer time, reducer concentration, and temperature are important to control the chemical synthesis and stability of Ag NP's, in addition the temperature plays an important role in controlling these parameters, therefore the nucleation and growth are important processes within the chemical synthesis of NP's. The formation of a nucleus implies an interface at the boundaries of a new phase. The temperature is the most important factor for the nucleation process[33]. Supercooling brings about supersaturation, the driving force for nucleation. Supersaturation occurs when the pressure in the newly formed solid is less than the liquid pressure, and brings about a change in free energy per unit volume, G_v , between the liquid and the newly formed solid phase. This change in free energy is balanced by the energy gain associated with forming a new volume and the energy cost due to the creation of a new

interface. When the overall change in free energy, ΔG is negative, nucleation is favored [33] [27]. Some energy is consumed to form an interface, based on the surface energy of each phase. If a nucleus is too small, the energy that would be released by forming its volume is not enough to create its surface, and nucleation does not proceed. The critical nucleus size can be denoted by its radius, and it happens when $r=r^*$ (or r critical) that the nucleation proceeds [34]. Figure 1 depicts the energy curves as a function of particle radius.

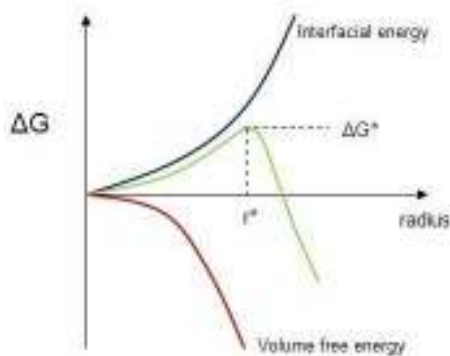


Figure 1 Critical Nucleus radius [33][34]

3.3 Oxidation-Reduction Method (Redox)

Redox (reduction-oxidation) reactions include all chemical reactions in which atoms have their oxidation state changed. It can be explained in the following terms, oxidation is the loss of electrons or an increase in oxidation state by a molecule, atom, or ion and reduction is the gain of electrons or a decrease in oxidation state by a molecule, atom, or ion[35]. In the redox synthesis, the reducer agent transfers electrons to the oxidant. Thus, in the reaction, the reducing agent loses electrons and is oxidized, and the oxidizing agent gains electrons and is reduced [35]. This method is used for the synthesis of nanoparticles. Currently, the size of nanoparticles is of interest for many applications and, as was mentioned in previous chapters, stability limits changes thus it could be used for controlling size.

3.4 Stability in colloids Ag NP's

Inorganic nanoparticles, such as silver, need to be stabilized against aggregation in aqueous environments. This may be conveniently accomplished by covering the surface of the nanoparticles with ionic charge groups [27]. A crucial aspect of colloid chemistry is the means by which the metal particles are stabilized in the dispersing medium to avoid agglomeration. At short interparticle distances, two particles would be attracted to each other by van der Waals forces which varies as the inverse sixth power of the distance between the particle surfaces [31]. Without the aid of any counteracting repulsive force, a sol would coagulate as shown in Figure 2. In general there are two methods for achieving counteraction: electrostatic and steric stabilization. [36] [37][10].

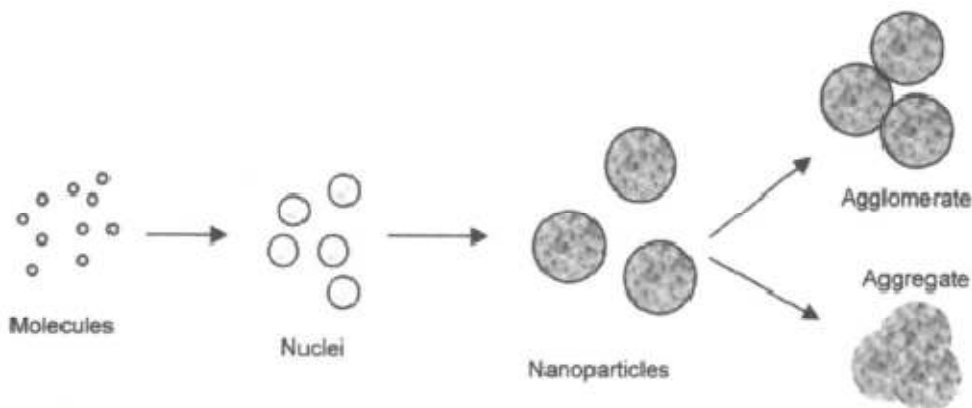


Figure 2. Difference between agglomeration and aggregate. [27]

3.5 Derjaguin, Landau, Verwey and Overbeek theory(DLVO theory).

The state of the NP's; isolated particles, aggregated or dissolved will vary depending on the environmental conditions (pH, ionic strength, presence of organic matter, etc.) [38]. Derjaguin, Landau, Verwey and Overbeek theory (DLVO theory) suggests that the stability of a colloidal system is determined by the sum of the van der Waals attractive (V_A) and electrical double layer repulsive (V_R) forces that exist between particles as they approach each other due to the Brownian motion. The energy barrier resulting from the repulsive force prevents two particles approaching one another to adhere

together. If the particles collide with sufficient energy to overcome that barrier, the attractive force will pull them into contact where they adhere strongly and irreversibly. Therefore, if the particles have a sufficiently high repulsion, the dispersion will resist flocculation and the colloidal system will be stable [39]. Flocculation is the formation of light, fluffy groups of particles held together by weak van der Waals forces [40]. However, if a repulsion mechanism does not exist then flocculation or coagulation will eventually take place. In certain situations (e.g. in high salt concentrations), there is a possibility of a “secondary minimum” where a much weaker and potentially reversible adhesion between particles exists.. These weak flocs (primary aggregated that may or not may sediment) are sufficiently stable not to be broken up by Brownian motion, but may dissociate under an externally applied force such as vigorous agitation. Therefore, to maintain the stability of the colloidal system, the repulsive forces must be dominant. There are two fundamental mechanisms that affect dispersion stability: steric and electrostatic repulsion, as can be seen in Figure 3: Steric repulsion involves polymers added to the system adsorbed onto the particles surface thus preventing the particle surfaces coming into close contact. If enough polymer is adsorbed, the thickness of the coating is sufficient to keep particles separated by steric repulsions, whereas if the van der Waals forces are too weak, it causes adhesion in the particles. The other mechanism is electrostatic or charge stabilization , which is the effect on particle interaction due to the distribution of charged species in the system [10][39] [11]. The following section presents the reagents used to obtain the stability by redox method.

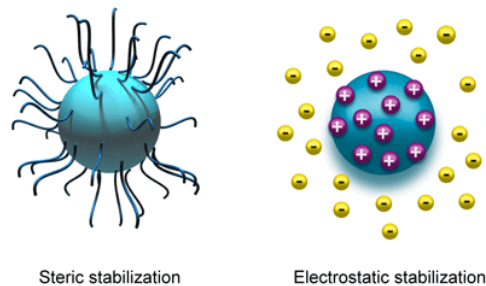
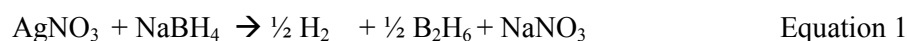


Figure 3 Types of colloidal stabilization[39]

3.6 Mechanism of formation for silver nanoparticles by redox method

The silver nanoparticles that were obtained in this work were synthesized by reduction of silver ions from silver nitrate salt (AgNO_3) using a sodium borohydride salt (NaBH_4) in DI degassed water with pH 7 (neutral). The dissociation occurred when both salts are mixed and the ions of Ag^+ , BH_4^- , NO_3^- , and Na^+ are obtained. Instantly, the borohydride ion (BH_4^-) reacted with the Ag^+ ions and reduced to Ag^0 (metallic silver) as described in the following reactions;[41][21]



Then,



and



The sodium borohydride lost an electron giving it to the silver in the aqueous solution after dissociation, then; the sodium borohydride is converted to borohydride anion. This anion acts as a ligand around the

surface of the metallic nanoparticle to produce the electrostatic effect. The (boranes) B_2H_6 are a weak acids, thus its pH avoid the positive superficial charge of the nanoparticle. By a slow rate hydrolysis of sodium borohydride the following reaction was formed [41][21][31]:



Where the metaborate ion is strongly basic, this pH allows a positive surface charge in the silver nanoparticle, then; the borohydride anion covers the silver NP surface by electrostatic effect. The basic pH allows to keep a slow rate of hydrolysis of borohydride anion until its full dissolution; however, enough amount of sodium borohydride is necessary for the chemical reduction, hydrolysis, and the electrostatic effect of borohydride around the silver nanoparticles. [35] [41][36]

In the case of the reduction of silver nitrate by sodium borohydride, the formed colloidal silver particles are surrounded by an electric double layer arising from the adsorbed borohydride ions and the cations which are attracted to them (an excess of sodium borohydride is essential for proper particle stabilization). This results in a Coulombic repulsion between the particles which decays exponentially with increasing interparticle distance. Thus, if the electric potential associated with the electrostatic repulsion of the double layer is sufficiently high, agglomeration is prevented. If too much sodium borohydride is added however, the overall ionic strength of the sol will increase leading to a compressed double layer and a shortened range of the repulsion. Ultimately the sol coagulates as the particles can no longer be kept apart [36]. This electric potential of the electric double layer can be measure as Z potential value.

In this work the responses of interest were the size of the nanoparticle, the Z potential, and the change of these responses with respect to time (as a quantified by the slope) as a measure of stability. The following section describes the statistical techniques use for the characterization of these responses.

3.7 The Experimental Design

A strategy of experimentation, that is used extensively, is the one-factor-at-a-time approach which consists of selecting a starting point, or a baseline set or levels for each factor. In this case all experiments are performed and a series of graphs are usually constructed showing how the response variable is affected by varying each factor with all other factors held constant. The principal disadvantage of this method is that it fails to consider any possible “interaction” between the factors. An interaction is the failure of one factor to produce the same effect on the response at different levels of another factor. Furthermore, the approach that considers any possible interaction of the factors is the factorial strategy in which the factors are varied together, instead of one at a time. In this kind of design the replicas in the center of the square are important to estimate the error. The data collected during this investigation was analyzed using MINITAB15. The analysis of variance (ANOVA) was used to quantify and evaluate the importance of possible sources of variation. It provides the basic information necessary for making statistical inference either in terms of tests of hypotheses (or tests of significance) or confidence interval estimation (F-test). The statistical results are interpreted in terms of the originally formulated hypotheses. A test of a hypothesis is a rule to determine whether a hypothesis is rejected or not and it is based on sample statistics called test statistics. Leardi et al. [42] showed the interest of applying experimental design techniques and a walkthrough in the chemical area. Their work can be related to the objective of this thesis. They presented three different case studies: (1) Application of a 2^k factorial design (2 levels, k factors) where the objective was to control the viscosity of a polymer. This experimental design is typically used when the interaction between two factors needs to be study along with the existence of curvature in the model. (2) Presents the application of the central composite design face centered in the analysis of copper milling process. This design is used to obtain predictions of second-order models. (3) Shows the use of a design of experiment analysis with mixtures, where a pharmaceutical company aims to develop a tablet

formulation. This publication demonstrated that the OVAT technique (One Variable at a Time), which means changing one factor at the time, is much less efficient than any of the techniques presented in the three cases [42].

3.8 Design of experimental process

Design of experiments (DOE) is a useful tool used when the source of variation of a specific system needs to be known. This variation depends on factors which may be significant in the system [13]. There is a wide variety of designs of experiment to choose from, therefore for selecting a specific design it is necessary to gain deep knowledge of the system and its specific response. This statistical tool provides the capability to develop a predictive model for the system based on the measurable response.

The selected approach for this work was the factorial design which is ideal when the exploration of the areas for the optimization of a particular response is desired. The first step is to identify critical parameters for our system. The following chart (Figure 4) shows a diagram with the factors affecting the synthesis of Ag nanoparticles.

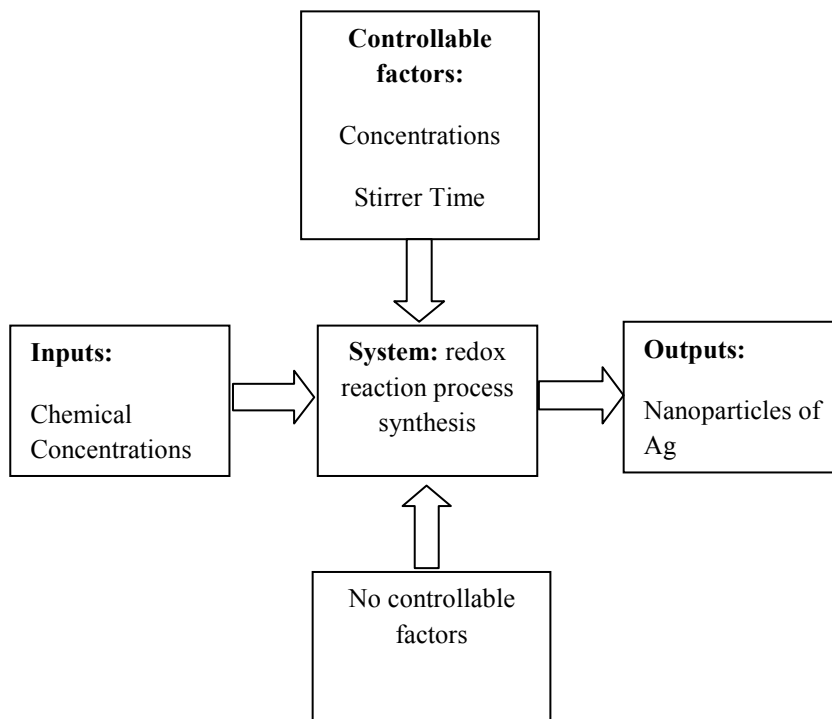


Figure 4.Synthesis process as a system.

From Figure 4 it is possible to see that there are a series of controllable factors, we chose three factors of interest for the synthesis process: reaction time, temperature of the reaction, and concentration of surfactant [17][19], as was presented in previous work.

A statistically designed experiment will efficiently and effectively answer questions of interest associated with the initial goal of a project. Factorial design, which is a kind of design of experiment is widely used in experiments involving several factors where it is necessary to study the joint effect of the factors on a response. The 2k design is particularly useful in the early stages of experimental work when many factors are likely to be investigated. It provides the smallest number of runs with which k factors can be studied

in a complete factorial design. Consequently, these designs are widely used in factor screening experiments.[13]

Because there are only two levels for each factor, it is assumed that the response is approximately linear over the range of the factor levels chosen. In many factor screening experiments, when an early understanding of the process or the system is needed, this is often a reasonable assumption.

3.9 The 2^3 Design

When there are three factors A, B and C, each with two levels, the design is called a 2^3 factorial design. The eight treatment combinations can be displayed geometrically as a cube, as shown in Figure 5 . Using the “+ and -” notation to represent the low and high levels of the factors, it is possible to list the eight runs in the 2^3 design [13].

Three different notations are widely used for the runs in the 2^k design. The first is the + and – notation, often called the geometric notation. The second is the use of lowercase letter labels to identify the treatment combinations. The final notation uses 1 and 0 to denote high and low factors levels, respectively, instead of + and -. These different notations are illustrated below for the 2^3 design. There are seven degrees of freedom between the eight treatments combinations in the 2^3 design. Three degrees of freedom are associated with the main effects of A, B and C. Three degrees of freedom are associated with interactions AB, AC and BC; and one with ABC. The following Figure 5 shows the coded levels for the three factors to be used in this work.

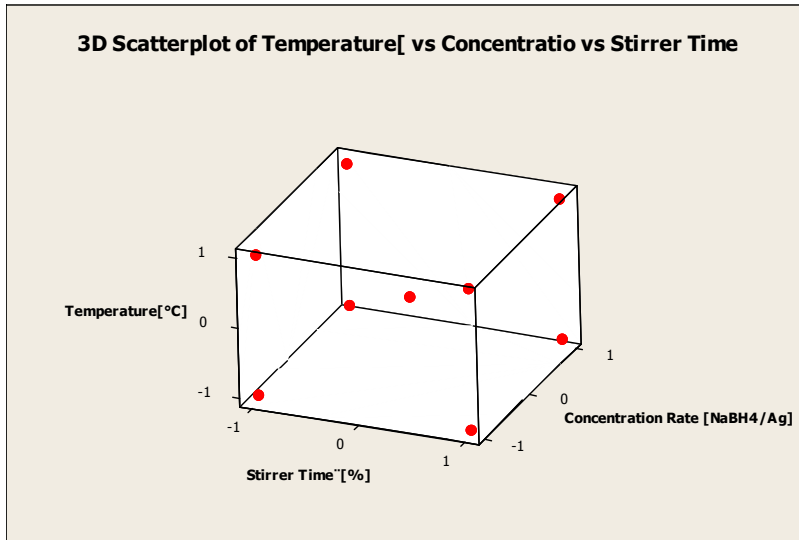


Figure 5. Points from a design of experiments 2³.

The main effect of A , when B and C are at low levels is $[a - (1)]/n$. Similarly, the effect of A when C is at the high level and C is at the low level is $[ab - b]/n$. The effect of A when C is at the high level and B is at the low level is $[ac - c]/n$. Finally, the effect of A when both B and C are at the high level is $[abc - bc]/n$. Thus, the average effect of A is just the average of these four, or

$$A = \frac{1}{4n} [a - (1) + ab - b + ac - c + abc - bc]$$

Equation 5

This equation can also be developed as a contrast between the four treatments combinations in the right face of a cube (where A is at the high level) and the four in the left face (where A is at the low level). That is, the A effect is just the average of the four runs where A is at the high level (\bar{y}_{A^+}) minus the average of the runs where A is at the low level (\bar{y}_{A^-}), or

$$A = \bar{y}_{A^+} - \bar{y}_{A^-} = \frac{a + ab + ac + abc}{4n} - \frac{(1) + b + c + bc}{4n} \quad \text{Equation 6}$$

This equation can be rearranged as

$$A = \frac{1}{4n} [a - (1) + ab - b + ac - c + abc - bc] \quad \text{Equation 7}$$

In a similar manner, the effect of B is the difference in averages between the four treatment combinations in the front face of the cube and the four in the back. This yields

$$\begin{aligned} B &= \bar{y}_{B^+} - \bar{y}_{B^-} \\ &= \frac{1}{4n} [b + ab + bc + abc - (1) - a - c - ac] \end{aligned}$$

The effect of C is the difference in averages between the four treatment combinations in the top face of the cube and the four in the bottom, that is,

$$\begin{aligned} B &= \bar{y}_{C^+} - \bar{y}_{C^-} \\ &= \frac{1}{4n} [c + ac + bc + abc - (1) - a - b - ab] \end{aligned}$$

The two-factor interaction effects may be computed easily. A measure of the AB interaction is the difference between the average A effects at the two levels of B . By convention, one-half of this difference is called the AB interaction.

Because the AB interaction is one-half of this difference,

$$AB = \frac{[abc - bc + ab - b - ac + c - a + (1)]}{4n} \quad \text{Equation 8}$$

The equation 8 can be written as follows:

$$AB = \frac{abc + ab + c + (1)}{4n} - \frac{bc + b + ac + a}{4n} \quad \text{Equation 9}$$

In this form, the AB interaction is easily seen to be the difference in averages between runs on two diagonal planes in the cube.

A potential concern of the use of two-level factorial designs is the assumption of linearity in the factors effects. Perfect linearity is unnecessary, and the 2^k system will work quite well even when the linearity assumption is barely obtained. In fact it is possible to note that if interaction terms are added to a main effect a first model result:

$$y = \beta_0 + \sum_{j=1}^k \beta_j x_j + \sum_{i < j} \beta_{ij} x_i x_j + \varepsilon \quad \text{Equation 10}$$

This model is capable of representing some curvature in the response function. This curvature, of course, results from the twisting of the plane induced by the interaction terms $\beta_{ij}x_i x_j$.

In some situations, the curvature in the response function will not be adequately modeled by Equation 10. In such case, a logical model to consider is

$$y = \beta_0 + \sum_{j=1}^k \beta_j x_j + \sum_{i < j} \beta_{ij} x_i x_j + \sum_{j=1}^k \beta_{jj} x_j^2 + \varepsilon \quad \text{Equation 11}$$

Where the β_{jj} represent pure second-order or quadratic effects. Equation 11 is called a second-order response surface model.

When executing a two-level factorial experiment, fitting the first-order model is anticipated, but we should be carefully with the possibility that the second-order model is more appropriate. There is a method of replicating certain points in a 2^k factorial that will provide protection against curvature from second-order effects as well as to allow an independent estimate of the error. The method consists of adding center points to the 2^k design. These consist of n_c replicates run at the points $x_i = 0$ ($i = 1, 2, \dots, k$). [13]

One important reason for adding the replicate runs at the design center is that center points do not affect the usual effect estimates in a 2^k design. When center points are added it is assumed that the k factors are quantitative.

3.10 P value and Determining Sample Size

The p value criterion was used in this work to determine whether to accept or reject the null hypothesis of equal variance in the responses of interest. The p value is defined as the minimum value of α , which would reject the null hypothesis when it is true. P value is analyzed with a confidence level of 95% (indicating the probability of not rejecting the null hypothesis when it is true) to have a significance value

of 0.05 ($\alpha = 0.05$). If the p value is less than α , the null hypothesis is rejected [13] [43]. The analysis of variance will be presented in the results chapter.

In any experimental design problem, a critical decision is the choice of sample size, that is, determining the number of replicates to run. Generally, if the experimenter is interested in detecting small effects, more replicates are required than if the experimenter is interested in detecting large effects. A methodology will be presented in next sections with the objective to select the optimum number of replicates.

4 MATERIAL CHARACTERIZATION TECHNIQUES

4.1 Preview

As was mentioned before, quasi-spherical nanoparticles are of interest in this work because they are poised to take advantage of the morphology and to obtain a specific surface area-to-volume ratio of the particle. Nanostructures with higher surface area-to-volume ratios are expected to favor the underlying sintering mechanism, and these structures are used for enhancing the performance of the sintering process used for electronic components because at this nanoscale, materials sinter at lower temperatures due to their larger surface areas relative to volume [18]. In previous work [44] it was demonstrated that for a good sintering process, it is necessary to have a combination of larger and smaller silver nanoparticles. This chapter describes the equipment used for the size characterization of the Ag nanoparticles. The techniques are described in the following order, first the Z sizer NanoS90 Instrument, then the Dynamic Light Scattering and X ray diffraction, and finally the Ultraviolet visible spectra.

4.2 The Z-Sizer NanoS90 Instrument

The Zetasizer Nano Instrument provides the ability to measure two characteristics of particles or molecules in a liquid medium, these are particle size and Zeta potential. By using specific technologies within the Zetasizer system these parameters can be measured over a wide range of concentrations. The Zetasizer features pre-aligned optics and programmable measurement position plus a precise temperature control necessary for reproducible, repeatable, and accurate measurements [12]. An image of this equipment is shown in Figure 6.



Figure 6. NanoS90 to measure of Z size and Z potential of Ag nanoparticles

4.3 Dynamic light scattering (DLS)

For characterization of Ag NP's, the DLS methodology was used to measure the hydrodynamic diameter of silver nanoparticles in water [38]. Particle size is the diameter of the sphere that diffuses at the same speed as the particle being measured. The Zetasizer system determines the size by first measuring the Brownian motion of the particles in a sample using Dynamic Light Scattering (DLS), and then interpreting a size from this measurement using established theories. Brownian motion is defined as “the random movement of particles in a liquid due to the bombardment by the molecules that surround them.”[12]. The particles in a liquid move about randomly and their speed of movement is used to determine the size of the particle. It is known that small particles move quickly in a liquid and large particles move slowly. This movement is carrying on all the time, by taking two “pictures” of the sample separated by a short interval of time, say $100\mu\text{s}$, it can be seen how much the particle has moved and therefore work out how big the particle is. If there has been minimal movement and the particle positions are very similar, then the particles in the sample will be large; similarly if there has been a large amount of movement and the particle positions are quite different, then the particles in the sample are small[12]. With DLS technique it was possible to characterize the size of the Ag NP's.

4.4 Zeta potential

The stability of nanoparticles in DI water was further determined by measuring zeta potentials of the particles (Malvern Instruments, Zetasizer Nano-ZS). Most liquids contain ions; these can be negatively and positively charged atoms called cations and anions respectively. When a charged particle is suspended in liquid, ions of an opposite charge will be attracted to the surface of the suspended particle. Negatively charged sample attracts positive ions from the liquid, and conversely, a positive charged sample attracts negative ions from the liquid. Ions close to the surface of the particle will be strongly bound while ions that are further away will be loosely bound, forming what is called a diffuse layer. Within the diffuse layer there is a notional boundary, and any ions within this boundary will move with the particle when it moves in the liquid; but any ions outside the boundary will stay where they are, this boundary is called the Slipping plane. A potential exists between the particles surface and the dispersing liquid which varies according to the distance from the particle surface, this potential at the slipping plane is called the Zeta potential. Zeta potential is measured using a combination of measurement techniques Electrophoresis and Laser Doppler Velocimetry, sometimes called Laser Doppler Electrophoresis. This method measures how fast a particle moves in a liquid when an electrical field is applied, its velocity. Once the velocity of the particle and the applied electrical field is known, by using two other known constants of the sample: viscosity and dielectric constant; the zeta potential can be worked out.

Zeta potential is a measure of the magnitude of the electrostatic, or charge repulsion attraction between particles in a liquid suspension. It is one of the fundamental parameters known to affect dispersion stability. Its measurement brings detailed insight into the causes of dispersion, aggregation or flocculation, and can be applied to improve the formulation of dispersions, emulsions and suspensions [45]. Therefore the Z potential value has been considered a possible means to characterize the stability in the Ag NP's.

4.5 X-ray Diffraction

This technique was used to determine the average crystallite size of the synthesized material. A wavelength of about 0.5 – 2.5 Armstrong is used for x-ray crystallography, in which the diffraction pattern produced by x-rays through the closely spaced lattice in a crystal is recorded and analyzed to reveal the nature of the lattice. Powder and thin films can be analyzed with this technique, using copper (Cu) radiation with a wavelength of 1.54 Armstrong is the one most often used in diffraction analysis. The wavelength attributed to Cu $k\alpha$ radiation is comparable to the atomic distance in a crystal, and is used for probing the structural arrangement of atoms in a wide range of materials. The x-rays provide information about the crystal structure. A crystal is constructed by the infinite repetition of identical structural units, and can be separated into the lattice and the basis. The basis is made up the simplest arrangement of atoms. Since each lattice point in the crystal has an identical environment, the basis is repeated at every point in the lattice to build up the crystal structure. A crystal lattice is a three-dimensional network of atoms that are arranged in a symmetrical pattern. When x-rays, electron rays, and neutron rays with the short wave length close to interatomic distance are applied to crystals, diffraction phenomena occur on the lattice planes in the crystals [11]. Diffraction patterns are formed by constructive interference of diffracted beams. The crystal structure is related to the incident beam by the Bragg's law [46].

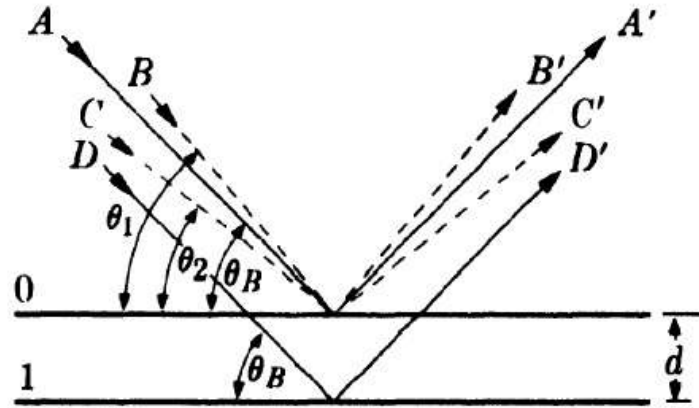


Figure 7. Diffraction phenomenon: A represent incident beam and A' represents diffracted beam [46]

This law describes the angle ($2\theta_{hkl}$) formed between the incident beam and the diffracted beams. This equation is:

$$n\lambda = 2d_{hkl} \sin \theta_{hkl} \quad \text{Equation 8}$$

λ is the wavelength of the incident radiation, d_{hkl} is a interplanar spacing, and is the diffraction angle. The average crystallite size may also be determined by means of the Scherrer's equation (below 100 nm): [16]

$$t = \frac{0.9\lambda}{B \cos \theta} \quad \text{Equation 9}$$

B corresponds to full width at half maximum of the broadened diffraction line on the 2θ scale in radians. The h , k and l letters are the Miller indices, which are a notation in crystallography for the planes and the directions in the crystal lattices [16].

The crystal structure analysis of silver nanostructures were carried out using the Cu-K α radiation and β Ni filter in a Siemens D500 powder x-ray diffractometer (Figure 8). XRD patterns were recorded in the 2 degrees range of $30^\circ - 90^\circ$ with a 0.02° step and a sampling time of 1 second.



Figure 8. X- Ray Diffractometer Siemens D50

4.6 Ultraviolet/Visible Spectroscopy (UV-vis)

UV radiation is the electromagnetic radiation of a wavelength shorter than that of visible light, but longer than that of x-rays. Colors may vary with objects, materials, light sources, etc., based on their physical properties such as light absorption, reflection, or emission spectra. Different materials may absorb light differently to show different colors. Many materials have an ability to absorb ultraviolet light, but human eyes are unable to detect it.

When a beam of monochromatic UV light, I_o passes through a solution, the optical transmittance T is defined as

$$T = I/I_o$$

Equation 10

Where I and I_0 are the UV light intensities before and after passing through the sample cell, as shown in Figure 3.4. The absorbance, A , is defined by:

$$A = \log(I/I_0) = \log(1/T) \quad \text{Equation 11}$$

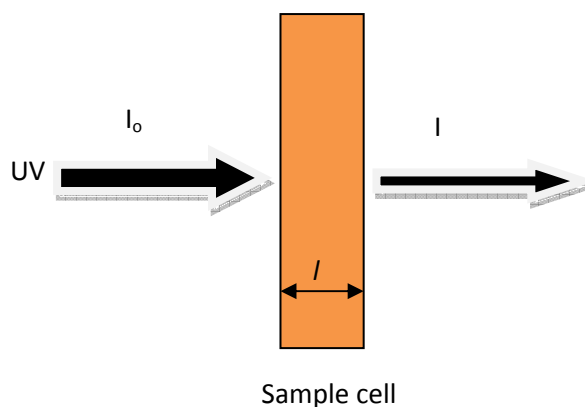


Figure 9. Sample Cell

The UV absorption A may follow the Beer-Lambert law. Absorbance (A) is directly proportional to the path length (l , cm) and the concentration (c , mol/L) of the absorbing species:

$$A = \epsilon lc, \quad \text{Equation 12}$$

Where ϵ is the molar extinction coefficient ($\text{L mol}^{-1} \text{cm}^{-1}$). ϵ is a measure of the amount of light absorbed per unit concentration. The Beer-Lambert law is valid only at low concentrations [47].

4.7 UV/Visible spectra

The molar extinction coefficient ϵ is not constant and often varies with wavelength λ . According to the Beer-Lambert law, at a fixed path length l , and a given concentration c , variation in ϵ with λ result in the variation of absorbance A . The variation of A with λ is called a spectrum. For a substance to have a

UV/Visible absorbance, it must be capable of being “excited” to move to a higher energy state (called “excited state”) from its ground state. [47]

A way to infer the silver nanoparticle size can be done in UV-vis by recording the changes in the intensity of the surface plasmon resonance (SPR) bands absorption which is expected to be seen in wavelength ranging from 397 to 410 nm where the silver nanoparticles has maximum absorbance when a surfactant is used [25]. The absorbance maximum is around 400-420 nm when the particles are polydisperse with sizes ranging from 10 nm up to 30 nm [48] [49]. This technique was used to characterize the absorbance peak for Ag NP’s from which the size of NP’s was inferred. An image of UV-vis equipment is shown in Figure 10.



Figure 10. Beckman Coulter DU 800 UV/Visible Spectrophotometer,

4.8 Plasmon in Ag NP’s

Nanoparticles of different sizes and shapes display different plasmon resonances, and as a consequence absorb light of different wavelengths, thereby giving rise to different colors of NP dispersions (Figure 11). Most commonly, synthesized silver nanoparticles are quasi-spherical particles with a plasmon resonance maxima around 400 nm and a characteristic yellow color [50] [48]. Ag NP’s are well known to have a

localized surface plasmon resonance (LSPR) peak, which causes a peak absorbance near 400 nm for unagglomerated particles, and shifts to longer wavelengths for agglomerated particles[14].

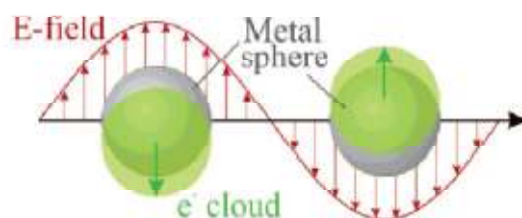


Figure 11. Schematic of the plasmon oscillation of a sphere [36]

5 EXPERIMENTAL PLANNING AND EXECUTION

5.1 Experimental Planning

This chapter presents the structure of the selected design of experiments, number of replicates, and the methodology carried out for the experimentation. Among the objectives of this thesis is the exploration and definition of an experimental area where stable NP's can be obtained. Towards this task it is first necessary to select the type of design of experiments to be used. This selection is critical because the structure of the design is what dictates its outcome. The selected design was a factorial design of experiments 2^3 , which enables the scanning of the zone as well as the definition of an optimal combination; additionally, one center point was added. As already discussed, the center points are important because they allow us to detect the presence of curvature in our data. After the structure of the design of experiments was selected, the number of replicates was determined. A starting point to select this number of runs is to specify the power value (P), which is equal to $1-\beta$, where P is the probability of correctly rejecting the null hypothesis (H_0) when it is false and β is the probability of failing to reject H_0 when this is false[13]. From this information, a small value of β and, thus, high value of P are desired. Motivated by the optimization of resources (chemicals reagents) and time (lab hours) three replicates were selected keeping a standard deviation value of 15. If three replicates are selected with a power value of 0.8 as illustrated in Figure 12 the projection in the x-axis is 18.14. This value can be interpreted as the minimum difference that can be detected for the values assigned to each response level, i.e. size and Z potential. The number of replicates was computed using Minitab Software version 15.

The effect value of 18.14 is slightly larger than the standard deviation of 15, but the power value of 0.8 was considered a good value to perform this experiment. As future work, after identifying the feasible zone for this synthesis a new structure of design of experiments will be proposed with the objective to improve the stability. To meet this, a composite central structure can be applied.

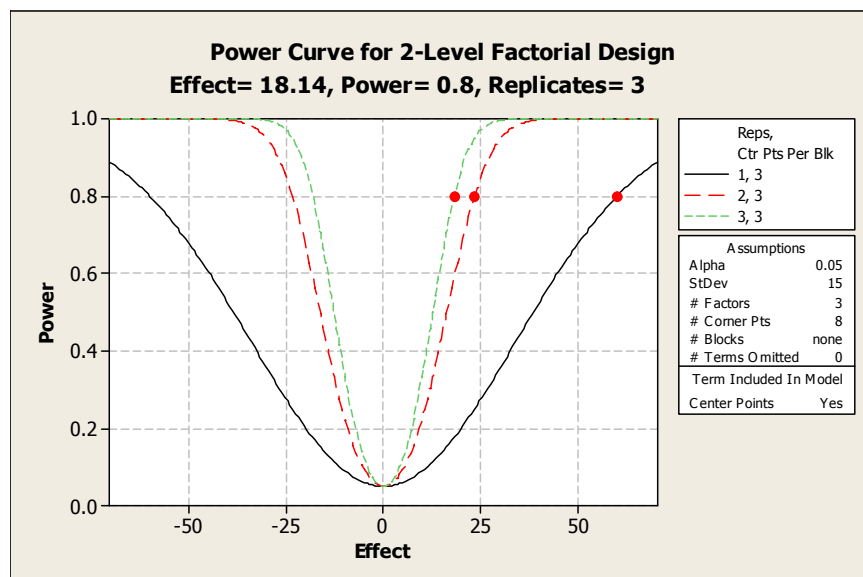


Figure 12. Power Curve to obtain the number of replicates

The experimentation was carried out with three factors with two levels and three replicates for each combination in addition to three center points for a total 27 runs. The selected factors were reaction temperature, stirrer time, and concentration rate. The reagents were silver nitrate (AgNO_3 , Sigma Aldrich, 99% purity), sodium borohydride (NaBH_4 , Sigma Aldrich, 99% purity), potassium hydroxide KOH (Sargent-Welch, 99% purity), ethanol, and DI water. The factor levels were: reaction temperature (0°C , 7.5°C and 15°C), stirrer time (50%, 100% and 150% of time), and concentration rate (R, 1, 12.5 and 26).

5.2 Experimental execution

The synthesis was elaborated by an oxide- reduction method which is the most common chemical route to obtain metallic silver. Degassed DI water (17 M Ω) at room temperature was used where a 50 mL aqueous solution containing silver nitrate (AgNO₃, 0.250 mM) and 150 ml of aqueous solution containing sodium borohydride (NaBH₄) was prepared in a 200 mL flask (which was varied to obtain different concentration rates ($R = \text{NaBH}_4 / [\text{AgNO}_3]$). This solution was kept at specific constant temperature using water chiller equipment. Afterwards the silver nitrate solution was added to the sodium borohydride solution employing a burette for drop frequency control of the synthesis, the burette was adjusted to the same rate for every sol synthesis (about 1 drop/sec). The synthesis time was around 18 minutes 30 seconds. The factors were set to the values presented in Table 1. The solution was stirred vigorously on a magnetic stir plate. A hot plate was used to keep the solution stirred at a constant speed (rpm) for specific intervals of time for all the samples. For each new trial the flasks were washed with an alcoholic potassium solution [14]. For all the experiments the aqueous solution for sodium borohydride was always renewed. Immediately after then synthesis the samples were characterized by UV vis spectroscopy, X Ray Diffraction, and Z sizer in order to obtain the size, Z potential values, and XRD pattern. All these values are necessary to determine the stability of the silver NP's. These measurements were taken at different times (hours and days) after the synthesis process completion. The first set of data was obtained in less than 60 minutes after the synthesis. The measurements were taken in the following order: “size 1 (or size at time 1)”, “Z potential 1” and then the UV Vis spectroscopy. After 72 hours (3 days), “size 2 (or size at time 2)”, “Z potential 2” and UV vis spectroscopy were measured for each combination, after that, the samples were kept in storage one week for observations. This interval of time was selected as first instance to capture the period of time where the NP's colloid are stable. The color of the NP's colloid was captured for all the combinations at time 1 and time 2. With these measurements from the DLS technique and ANOVA analysis the statistical models for the prediction of size and Z potential were obtained. From

the ANOVA it was possible to identify the significant factors for the chemical synthesis. The stability parameter in the colloid of NP's was measured by two parameters (i) changes of the size values measured from time 1 to time 2 (slope), and(ii) the change of the Z potential values from time 1 and time 2. The stability parameter can be a negative or positive value, in the case of positive values, it indicates a reduction in size or Z potential values, in the case of negative values, it indicates a reduction in the size or Z potential values. As it is known, flocculation and gravity force effects were acting on the NP's colloid, therefore this dynamic scenario make it only possible to capture the values of the sizes and Z potentials at the instant the particles were suspended in the center of 200 ml flask [10][11].

Table 1. Level factors for the experiment design

Controllable Factors	Levels
Reaction Temperature (°C)	0, 7.5 and 15
R= ([NaBH4]/[AgNO3])	1,12.5 and 26
Stirrer Time (sec)	From 50% , 100% and 150% of the synthesis time

The following flow chart on

Figure 13 shows the methodology for the synthesis used in this work applying the factorial experiment 2³.

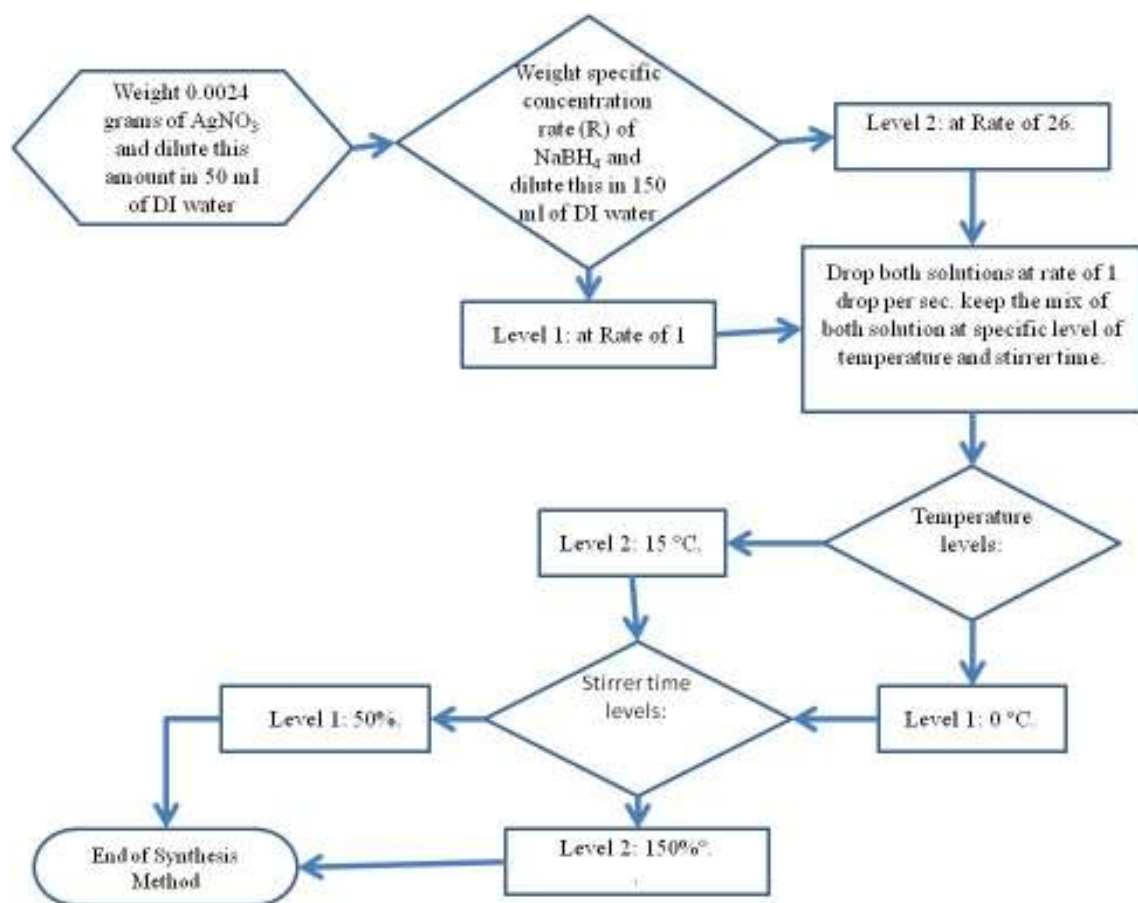


Figure 13. Methodology for the synthesis used in the experiment

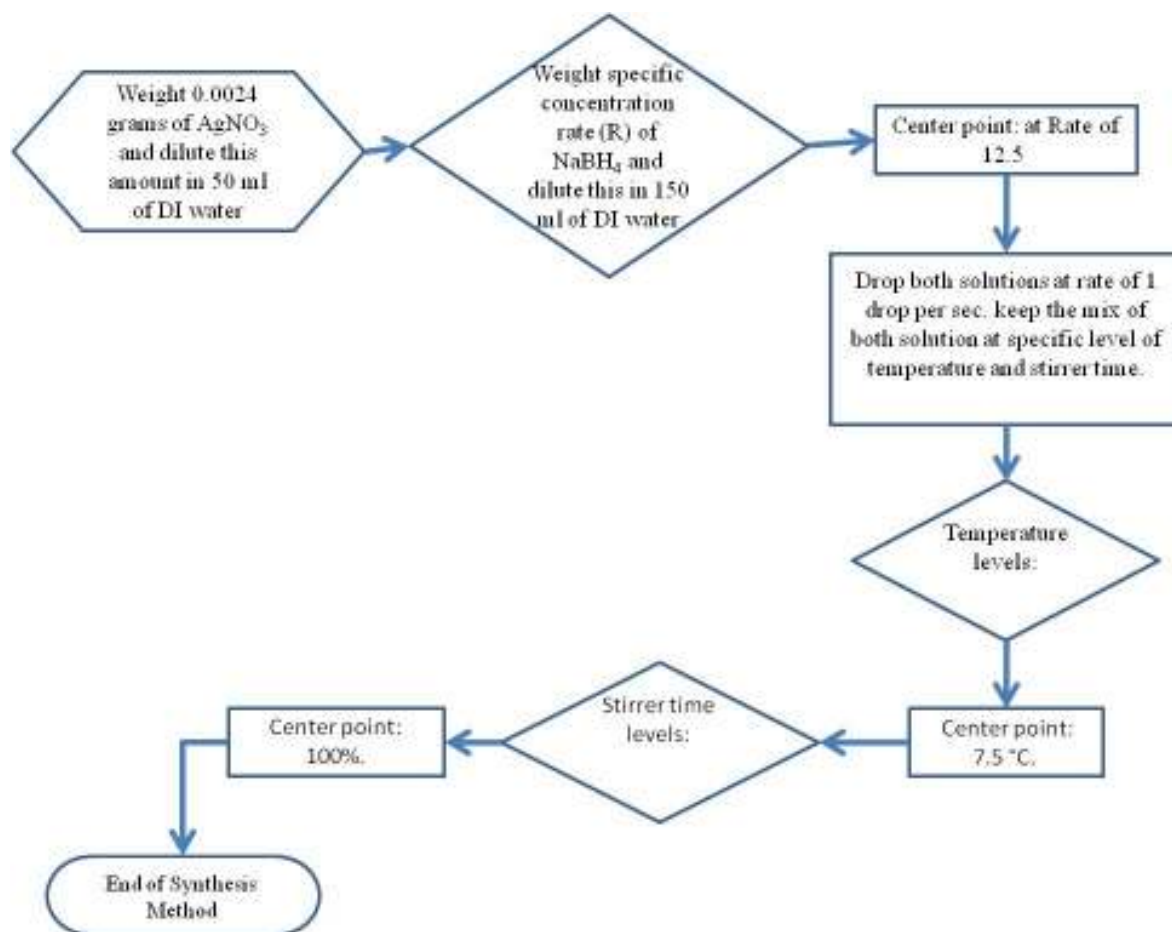


Figure 14. Methodology for the synthesis used in center point

The following chapter presents the results and discussion for this work. The ANOVA p values, scatter plots, XRD patterns, color images, and UV vis spectroscopy are discussed.

6 RESULTS AND DISCUSSION

6.1 Introduction

In this chapter the results and the discussion of the experiments that were carried out are presented. The experimental conditions, amounts, and code of each sample are shown in the Table 6 in the

APPENDIX A . From each trial, a colloidal system of metallic Ag was obtained and characterized by the techniques described in Chapter 3. The first section (6.2) presents the results from the interval plot graphs for all trials, then a specific combination (trial) was used in next sections to explain the rest of the analysis, i.e. the 24 trials (8 combinations with 2 replicates, 27 in total). The following sections (6.3 to 6.5) discuss the results for sample M1-115150, except section 6.7, which discuss the remaining samples from a point of view of color and UV-vis plasmons. Section 6.7 discusses the factors and their effect in the synthesis process. The sample code was divided as: M1-1-15-150 to explain the meaning for each

letter and number. The letter M represent “sample” and the number that follows this letter represent the replicate number, in this case, the first trial or first replicate for each combination. The first number is the concentration rate, the second number represents the temperature level, and finally; the third number represents the stirrer time percentage. With this information it is easy to identify that the factors’ levels in this case were 1 for the concentration rate (R), 15 °C for the temperature, and 150% for stirrer time.

The rest of results are presented as follow: the APPENDIX B shows the second part of Interval plots for all the trials, the APPENDIX C shows the color Analysis and the APPENDIX D shows the UV-vis results for the rest of 24 combinations. The APPENDIX E presents the residuals analysis for ANOVA for all the combinations. As it was mentioned in chapter 3, the stability of the colloid Ag system is the main objective in this work, and this behavior can be estimated by the agglomeration effect. In this work the agglomeration was measured from the parameter “*slope*”, which was explained in chapter 3. The agglomeration was also inferred from the interval plot graphs together with the colloid color and UV vis spectroscopy results.

6.2 Interval plots analysis

In this section the interval plots graphs obtained from the designs of experiments are presented. The responses of interest in these graphs were the average for *size 1*, for *size 2* and for the *z potential slope* values for the silver nanoparticles, from varying the three factors at time: reaction temperature (°C), stirrer time (% of time), and concentration rate (R). The interval plots were obtained using Minitab V15 software using the bonferroni technique [14]. This technique estimates a median value of the response for each factor level in order to obtain a confidence interval of 95%, with the limit that this confidence interval does not have the parameter with a probability of 0.05.

6.2.1 Interval plot for the average size 1, size 2 and Z potential slope

The interval plot shown in Figure 15 presents the confidence interval for the average values of “*size 1*” for the Ag NP’s, this response was plotted by varying the three factors selected in this work. The x-axes in the plot have the factors levels and the y-axes have the values of *size 1* for each combination.

The variation in concentration rate (R) factor, from 1 to 26, showed a significant difference between the values of *size 1*. The smallest average value of *size 1* was 5.14 nm, when the lower level of R was used, whereas the largest average value was 127.11 nm corresponding to the higher concentration level. The difference between these values is larger than the average of the standard deviation cited in literature (15 nm) [14], also a significant difference (larger than standard deviation) was found between both values, when compared with the average value of 27.86 nm for the center point level (R=12.5). The dispersion (variation) for the each confidence interval values for all the runs was found to be small. *Size 2* values are shown in Figure 15 from where it is possible to see that these responses changed from 5.14 nm to 4.61 nm, 127.11 nm to 3.61 nm, and 27.86 to 3.34 nm respectively.

Variations in the levels, for the temperature factor, showed (Figure 15) that there are significant differences between the values of *size 1* only for the samples elaborated at a high level of the concentration rate. It is possible to note that for the level 0°C and 15°C the values of sizes 1 were 54.83 nm and 127.17 nm respectively, and for the center point (7.5°C) the value was 27.86 nm. The *size 2* plot showed that the values changed from 54.83 nm to 27.26nm, 127.11 nm to 3.61 nm, and 27.86 to 3.34 nm for each of the respective experimental trials.

Stirrer time variations also showed significant difference between the average of *size 1* only when the high level of concentration rate factor was used, moreover it is possible to see that for the 50% and 150% level, values of 127.17 nm and 37.95 nm were obtained respectively. For the center point (100%) the response was found to be 27.86 nm. The *size 2* plot showed that the *size 1* value changed from 37.95 nm to 63.36 nm

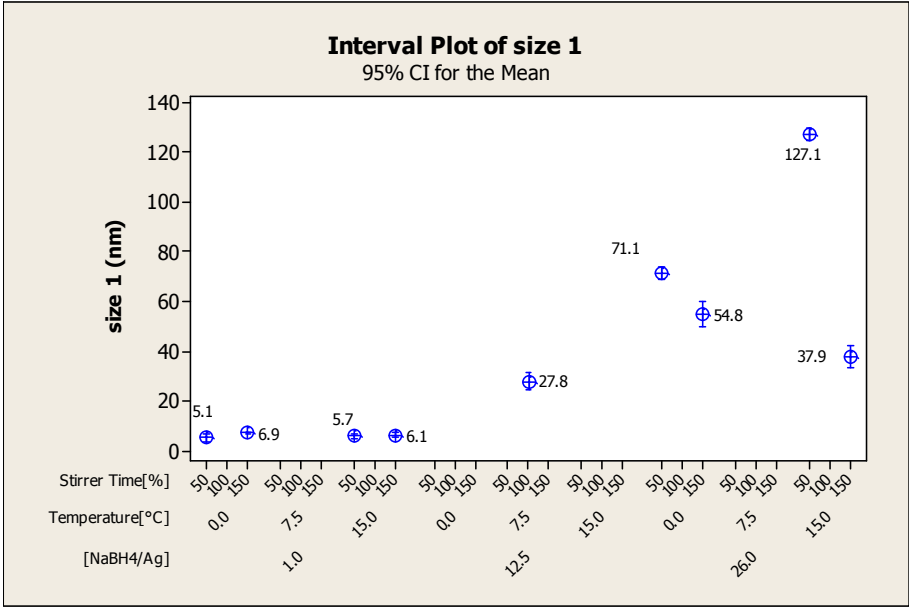


Figure 15. Interval plot for size 1

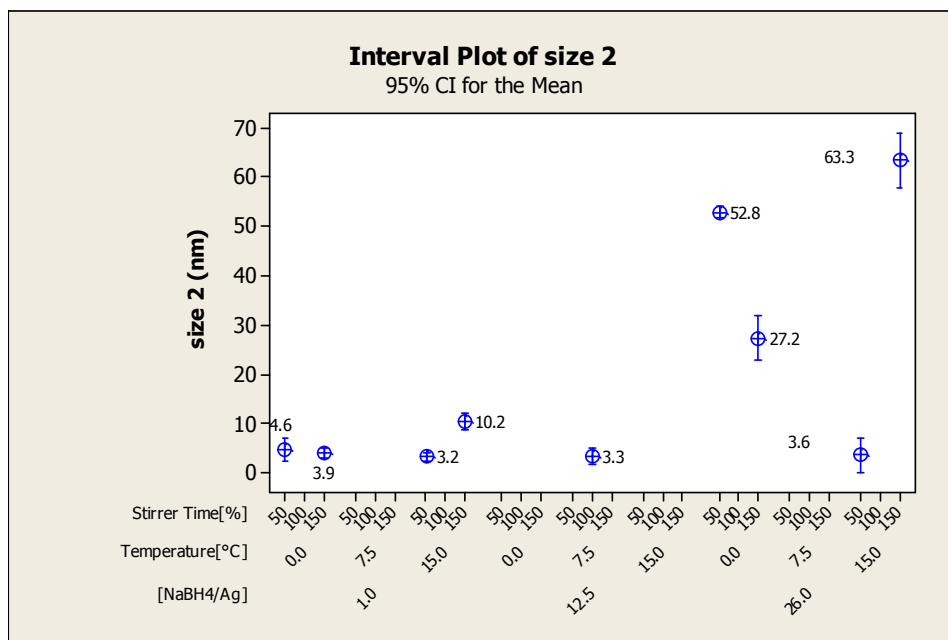


Figure 16. Interval plot for *size 2*.

The average values for the *size slope* of all the runs can be seen in the Figure 17 from which a significant change in this response (slope of -1.71) can be observed when compared with the rest of the trials that resulted in values ranging from 0.38 and -0.38. There is also a marked difference between the slopes for the samples that were synthesized with a high level of the concentration rate.

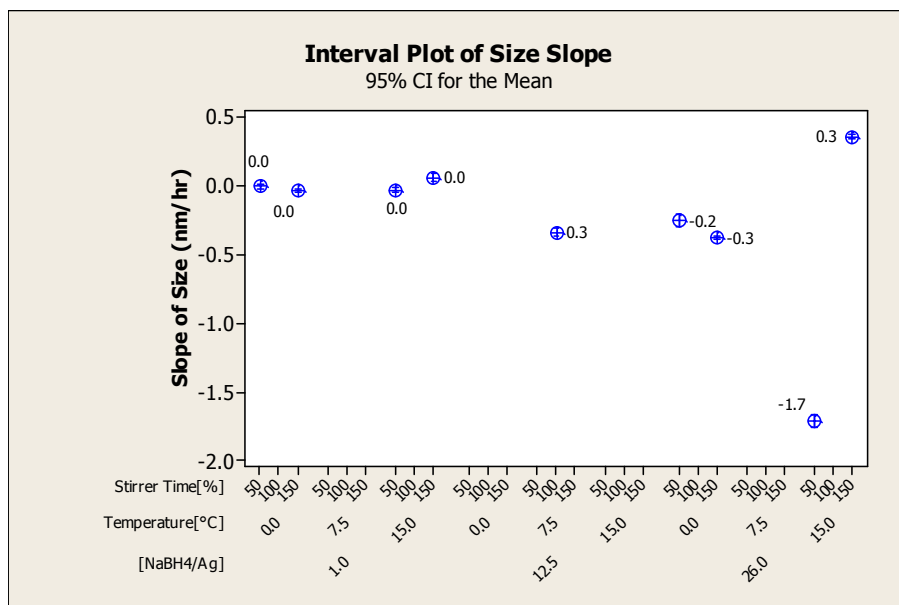


Figure 17. Interval plot for *size slope*

6.2.2 Interval plots results for z potential slope values

Values of *z potential slope* are given in Figure 18, whereas the values of z potential 1 and 2 are presented in the APPENDIX B (Figure 40 and Figure 41). From the graphs of the z potential 1 and 2 it can be seen that there exist a large dispersion in the results. In z potential 1, the combinations: M-12.5-7.5-100, M-26-0-50 and M-26-0-150 did not show a large dispersion when compared with the other six trials. For the z potential 2, the combinations: M-12.5-7.5-100 and M-1-0-150 did not present large dispersion in the interval of confidence if compared with the rest of the samples. For *z potential slope* values the samples: M-1-0-50, M-12.5-7.5-100, M-26-0-150, M-26-15-50 and M-26-15-150 did not result in large dispersion within the interval of confidence for this response as compared with the rest of the samples.

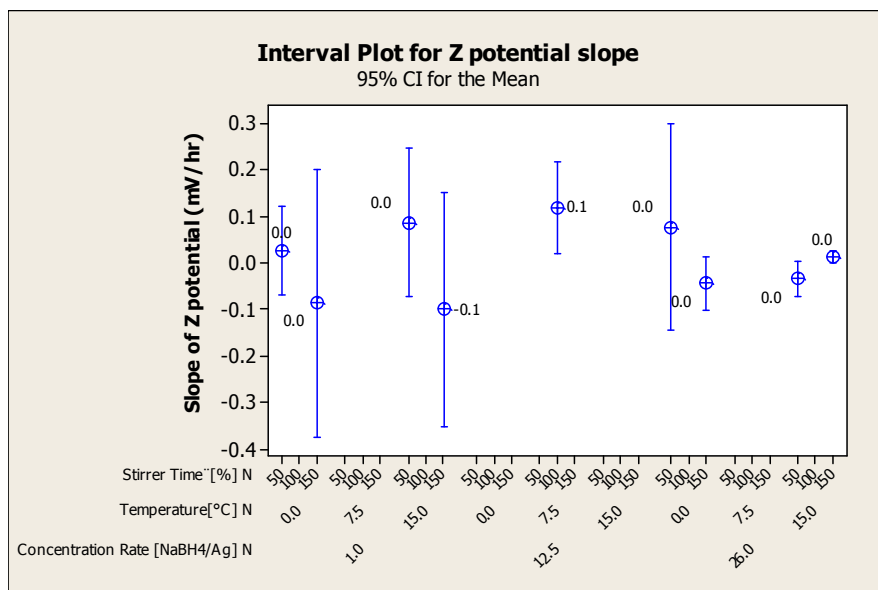


Figure 18 Interval plot of *z* potential slope

Z potential values around 30 mV [11] are known to be indicative of colloid stability, however due to the uncertainty of the test associated with the concentration of the sample and the resulting variability of the measurements, it was concluded to not use these z potential results in discussing the stability of Ag colloid.

6.2.3 Discussion for the interval plots

From our results, it was found that there is a significant difference in *size 1* and *size 2* values when the highest and lowest levels of the sodium borohydride concentration are used. From literature it was expected that large Ag NP's should result when high levels of borohydride are used, whereas for low concentrations smaller sizes should result. Size variations of the experimental concentrations rates resulted to be larger than the selected standard deviation values for this work (i.e. 18 nm). Inspection of the variation in the size slope for samples synthesized at the lower level condition proved what is

mentioned in literature. Small sizes were expected for low temperature conditions [14][21][31], however, from our results, this effect was not observed when high levels of concentration rate and low temperatures were used, moreover small sizes were in fact obtained at low levels of concentration rates and low temperatures. It can be inferred that the expected small size for all low temperature level (0°C) combinations was not present in the colloids due the high concentration rates used. This condition allows for the reduction of all the silver nitrate thus the agglomeration in the particles start to occur. When 100% stirrer time was used it can be seen that a slow agglomeration occurs. From literature it is known that this effect should be present after several weeks or months [14] when low temperatures (0°C), sodium borohydride concentration rate of 2:1, and 100% stirrer time are used. The effect of slow agglomeration can be attributed to the homogeneous distribution of the borohydride anions (negative charge ions) around the Ag nanoparticle which can be achieved by the constant agitation of these ions during the total time of the synthesis process hence avoiding agglomeration. Also, it was possible to observe that for low levels of stirrer time, the values of *size 1* were larger than the values obtained with the high levels of this factor. This effect can be influenced by the high concentrations rate factor used where the difference between *size 1* response was large than 18 nm.

In general, from observations of the plots, a significant decrease of *size 1* to *size 2* was obtained for some combinations, specifically in those synthesized with high levels of concentration rates. This change may suggest that there is shrinkage of the NP's; however this is an artifact of the micro flocculation mechanism. The micro flocculation effect allows the agglomeration of the nanoparticles which results in the formation of larger aggregates that owing to gravity tend to precipitate as sediment. Therefore, with time, those larger structures are not longer suspended in the colloid thus impossible to be detected by our characterization method which samples out from the central area of the colloid flask. Based on this fact, only smaller (non flocculated) particles will be suspended therefore causing an apparent decrease in size which is nothing but the result of a natural screening mechanism. Based on this analysis, what becomes critical in defining the stability of the system is the absolute value of the rate of change in size; i.e. the

size slope. Small values of the slope suggest minimal change in particle size hence stability, whereas a large slope (positive or negative) is an indicator of instability. It has been published that with high concentration rates of sodium borohydride the nanoparticles tend to agglomerate in short intervals of time [21]. From our results, it can be concluded that the concentration rate, stirrer time and temperature factors were significant for the synthesis of Ag NP's.

6.3 Colloid color analysis (Qualitative analysis)

In this section the color images for sample M1-115150 are presented from time 1 to time 2 (Figure 19 and Figure 20). It can be seen that for the replicate there was not a discernible change in the color of the colloid. This sample held the shiny yellow color from time 1 to time 2. The shiny yellow indicates that the colloid has metallic Ag nanoparticles while the dark yellow or dark brown color indicates that agglomeration had occurred [14][31]. The second replicate (see Figure 21 and Figure 22) did not present a significant color change from time 1 to time 2. In this sample the concentration rate was at the low level, from literature it is known that a ratio of 2:1 is necessary in the synthesis to ensure that all the silver nitrate becomes metallic silver nanoparticles. There is a probability that all the silver nitrate did not become metallic silver in this sample (M1-115150) since the R was set to 1. In the third replicate (see Figure 23 and Figure 24) it was possible to observe that the shiny yellow color in the colloid was kept from size 1 to size 2 as well. This effect can be explained from the plots for size 1 and size 2 presented in Figure 15 and Figure 16 (for low levels of R), where the values did not present a significant change along time. This could be associated with the fact that the amount of synthesized metallic silver nanoparticles was small and there was a large separation between nanoparticles, thus, the agglomeration effect was not present. The Ag colloids systems that did precipitate (agglomeration after five days) were identified in Table 6 in

APPENDIX A from where it is possible to see that the samples which presented agglomeration were from the combinations with levels of 50% and 150% of stirrer time.

<p>a)</p> 	
<p>Figure 19. Color of solution for combination M1-115150 at time 1</p>	<p>Figure 20. Color of solution for combination M1-115150 at time 2</p>

<p>b)</p> 	
<p>Figure 21. Color of solution for combination M2-115150 at time 1</p>	<p>Figure 22. Color of solution for combination M2-115150 at time 2</p>

<p>c)</p> 	
<p>Figure 23. Color of solution for combination M3-115150 at time 1</p>	<p>Figure 24. Color of solution for combination M3-115150 at time 2</p>

6.4 Ultraviolet-visible (UV-vis) spectroscopy analysis (Qualitative analysis)

The following UV-vis graphs (Figure 25 and Figure 26) for sample M115150 showed a slight decrease in the height of absorbance peak value from the time 1 to time 2 (0.14 to 0.10). Blue shift in the plasmons was observed from 395 nm to 385 nm respectively. The blue and red shifts in the UV-vis plasmons values indicate decrease and increment in the particle size respectively [50]. In this sample, the blue shift, indicated decrease in the nanoparticle size, which can be attributed to the microfloculation, although this effect cannot be seen in the color images. Wide peaks in UV- vis indicates the absence of monodispersion in the size of Ag NP's.

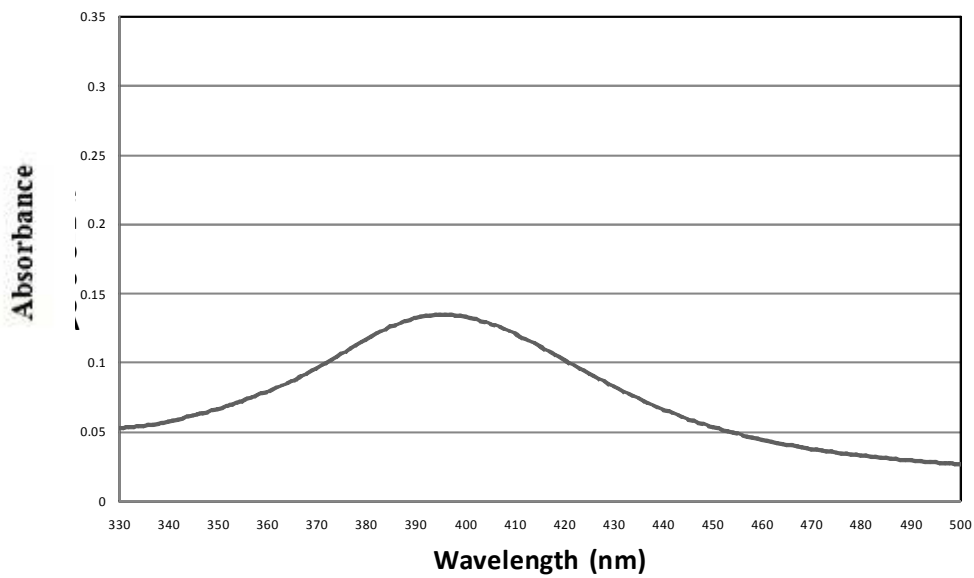


Figure 25. UV vis spectroscopy for the sample M1-115150 at time 1

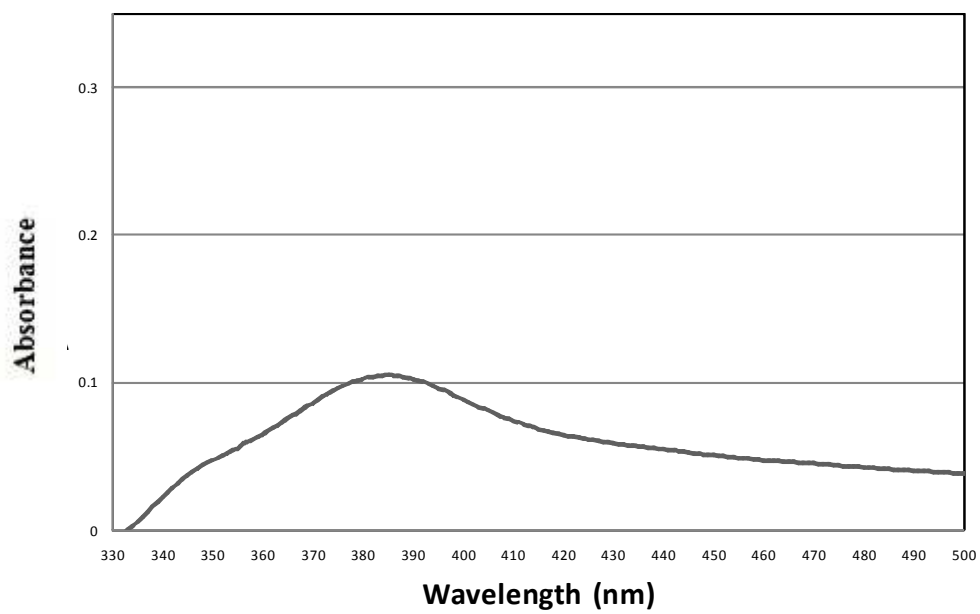


Figure 26. UV vis spectroscopy for the sample M1-115150 at time 2.

X Ray Diffraction Analysis

From all the XRD patterns obtained for each of the eight experimental conditions, it was possible to confirm that in all instances metallic silver was attained as shown in

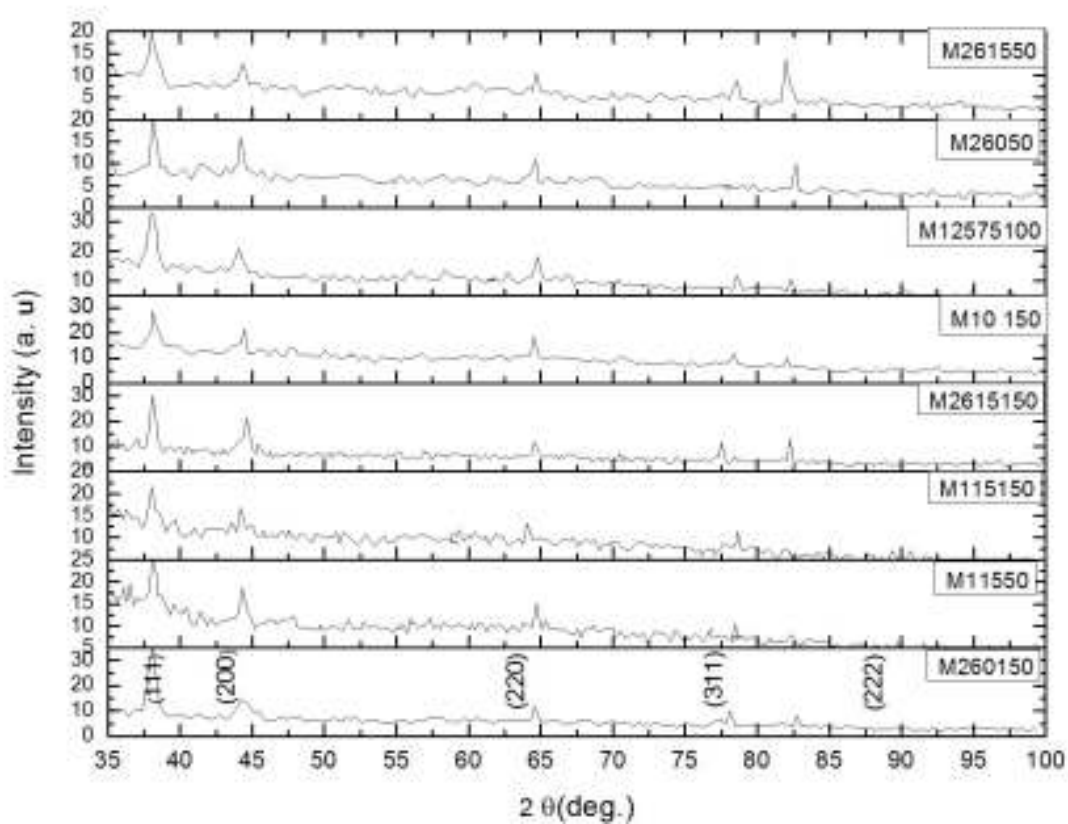


Figure 27 .

Figure 27. XRD patterns for the eight samples of Ag NP's

6.5 Statistical Analysis (ANOVA)

This section presents the ANOVA for *size 1*, *size 2* and *size slope* for all the samples synthesized in this work. The residual analysis is presented in APPENDIX E.

6.5.1 The p value for the average sizes and slope

The p values, when the factors were varied, for the sizes 1 and 2 are given in Table 2 and Table 3. These results demonstrated that all the factors and their interactions had a statistically significant (p values smaller than 0.005) effect on *size 1* during the synthesis process. As given in Table 3 it was found that all of the selected factors had also a significant effect on *size 2*. In Table 4 it is demonstrated that the factors of interest were pivotal in defining the size slope. Data on these tables confirm what was usually detected in the inspection of the interval plots in which a clear difference between size and slopes were observed.

Table 2. ANOVA results for *size 1*

ANOVA results for <i>Size 1</i>		
Term	P value	Coefficients
Constant	~0	39.38
Concentration Rate [NaBH ₄ /Ag]	~0	33.39
Temperature[°C]	~0	4.86
Stirrer Time [%]	~0	-12.91
Concentration Rate [NaBH ₄ /Ag]*Temperature [°C]	~0	4.9
Concentration Rate [NaBH ₄ /Ag]*Stirrer Time [%]	~0	-13.47
Temperature[°C]* Stirrer Time [%]	~0	-9.27
Concentration Rate [NaBH ₄ /Ag]*Temperature [°C]*Stirrer time [%]	~0	-8.94

Table 3. ANOVA results for *size 2*.

ANOVA results for <i>Size 2</i>		
Term	P value	Coefficients
Constant	~0	21.14
Concentration Rate [NaBH ₄ /Ag]	~0	15.63
Temperature[°C]	~0	-1.01
Stirrer Time [%]	~0	5.06
Concentration Rate [NaBH ₄ /Ag]*Temperature [°C]	~0	-2.26
Concentration Rate [NaBH ₄ /Ag]*Stirrer Time [%]	~0	3.49
Temperature[°C]* Stirrer Time [%]	~0	11.63
Concentration Rate [NaBH ₄ /Ag]*Temperature [°C]*Stirrer time [%]	~0	9.7

Table 4. ANOVA results for *size slope*.

ANOVA results for <i>Size slope</i>		
Term	P value	Coefficients
Constant	~0	-0.25
Concentration Rate [NaBH4/Ag]	~0	-0.24
Temperature[°C]	~0	-0.08
Stirrer Time [%]	~0	0.24
Concentration Rate [NaBH4/Ag]*Temperature [°C]	~0	-0.09
Concentration Rate [NaBH4/Ag]*Stirrer Time [%]	~0	0.23
Temperature[°C]* Stirrer Time [%]	~0	0.29
Concentration Rate [NaBH4/Ag]*Temperature [°C]*Stirrer time [%]	~0	0.25

6.5.2 Statistical model

The next step in the statistical analysis was to determine the input variable settings that would produce silver nanoparticles meeting specifications for the desired size and stability. Least squares regression is commonly used to estimate the coefficients of a linear model relating a response to the experimental factors in a designed experiment. As all the p values were significant for size and slope it was possible to obtain a statistical model from its coefficients (see Table 2 and Table 3) as given by each ANOVA analysis.

The analysis yielded the following equations (models), which can be used to predict *size* and *size slope* values for this process synthesis condition of interest. The model variables were Rate (R), Temperature (T) and stirrer time (St). From the previous analysis it was concluded to not consider the model for *Z potential* values, therefore the *Z potential* Model is not presented in this section. The statistical model to estimate the size is a function of synthesis parameters as follows:

$$Size1 = 39.38 + 33.39(R) + 4.86(T) - 12.91(St) + 4.9(R)(T) - 13.47(R)(St) - 9.27(T)(St) - 8.94 / R(T)(St)$$

The statistical model to estimate the *size slope* is given by:

$$SizeSlope = -0.25 - 0.24(R) - 0.08(T) + 0.24(St) - 0.09(R)(T) + 0.23(R)(St) + 0.29(T)(St) + 0.25(R)(T)(St)$$

Figure 15 and Figure 16 shows the change of sizes by the time, and it is important to note from Figure 17 that with negative or positive significant slopes there is not stability in the Ag NP's colloid. Residuals plots were used to confirm the adequacy of the model fit and ensure the least squares analysis assumptions were met.

Using these equations it is possible to determine a set of processing conditions to synthesize Ag NP's colloid with specific size and stability characteristics (*size slope* values) within the capacity of the studied synthesis process. In addition, these models help identify the critical inputs that needed to be tightly controlled in order to keep the size stable over time.

The following figures show the contour plots obtained from the statistical models. From these contour plots a feasible region for the synthesis of small silver NP's at time 1, as well as the best combination for particle's stability was found. Figure 28 shows the region (dark blue area) where it is possible to obtain small values for *size I* (0 to 20 nm) at low concentrations settings (R), and with temperatures ranging from 0°C to 15°C at a stirrer time fixed at 50%. It is possible to observe that controlling the concentration rate (R) to values below 5 results in small values of *size I* (0 to 20 nm). From the contour plots it was found that the variation of temperature does not significantly affect *size I* values when the stirrer time was kept at 50%. Furthermore, when the concentration of borohydride increases the *size I* value increases as well.

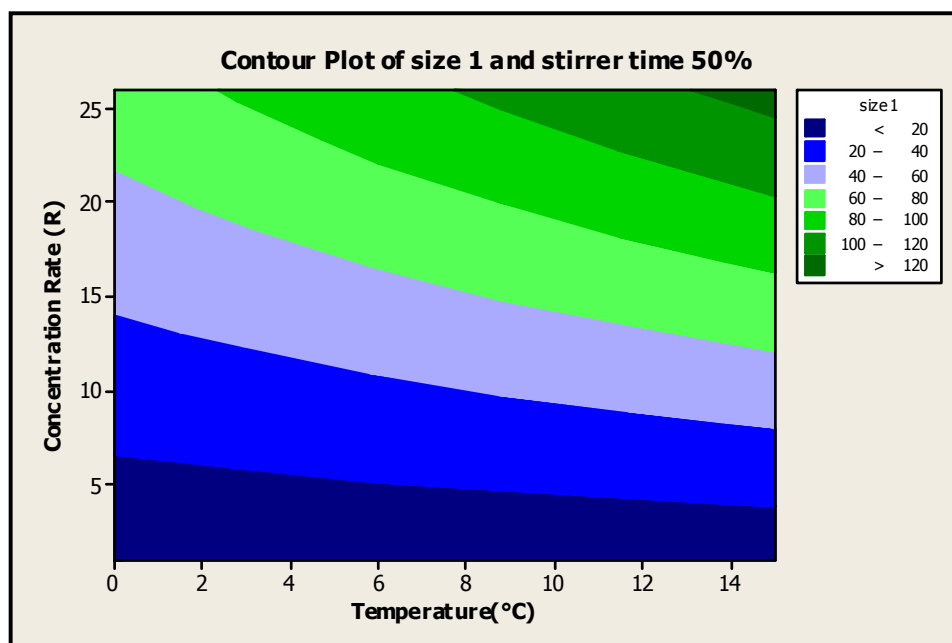


Figure 28. Contour plot for *size1* at stirrer time 50%

Figure 29 depicts the region (darker green area) where small values of *size slope* (close to zero), i.e. stability, could be obtained from the synthesis. For example, by inspection we can conclude that a stable colloid would result if the synthesis is performed at around 0° C while using a concentration rate from 1 to 20. Moreover, at low concentrations, i.e. rate of 5, combined with a temperature range from 0° C to 15° C small values of *size slope* (close to zero) are expected for stirrer time fixed at 50%. At concentration rates below 5 the variation of temperature has not a significant effect in the stability of the system. As expected with complex system, there exists another experimental zone where it is possible to obtain stability as measured from *size slope*, that is when concentration values range from 5 to 15 and the

temperature is set between 0 °C to 3°C. In general, when the concentration of borohydride increases (above 5) the *size slope* increases with the variation of the temperature thus lack of stability results.

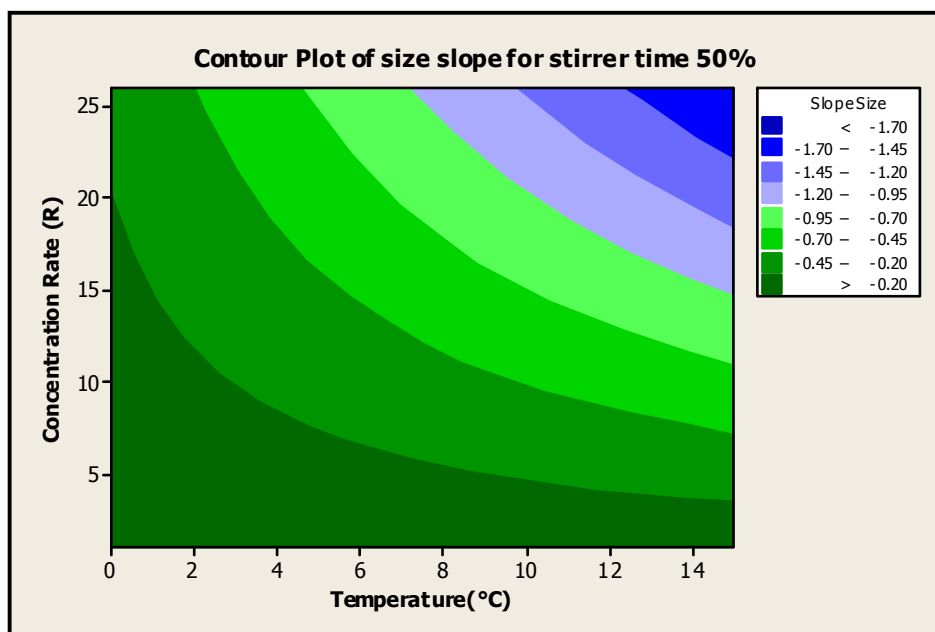


Figure 29. Contour plot for *size slope* at stirrer time 50%

Figure 30 presents an experimental region (light green area) where it is possible to obtain small values of *size I* (0 to 10 nm) through this synthesis. From our work it can be suggested that at low concentrations (R~ 1-3) and the temperature ranging from 0°C to 15°C, for a fix stirring time of 150% small particles shall result. It was also found that when the concentration rate (R) is controlled to values below 5 smaller values of *size I* (0 to 10 nm) will result when compared to higher rates values. It is critical to note that the temperature variation has not a significant effect on *size I* when the stirrer time was kept at 150%.

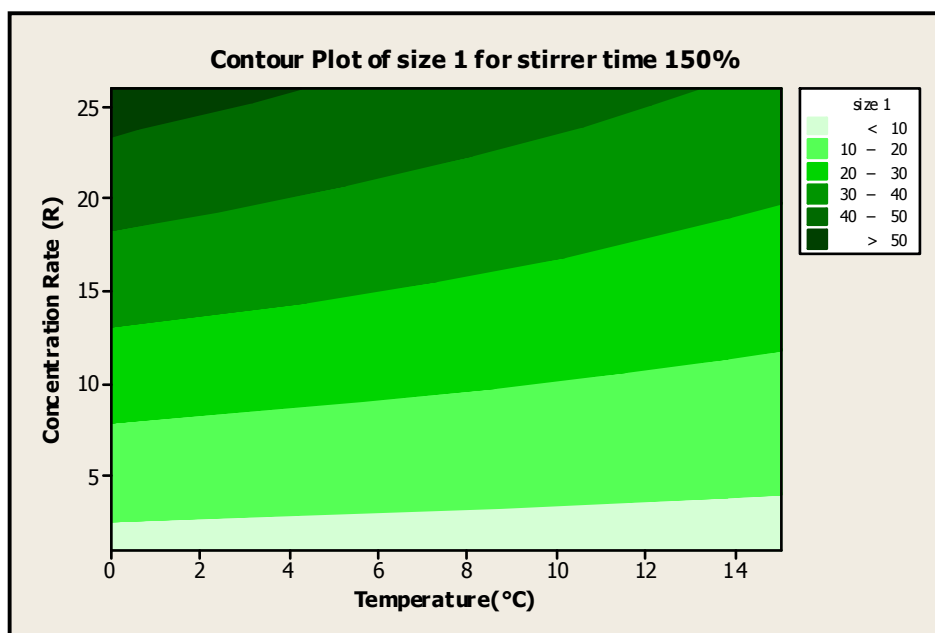


Figure 30. Contour plot for *size1* at stirrer time 150%

Figure 31 depicts the experimental region (light blue-gray and light greens areas) where it is possible to get colloid stability as measured small values of *size slope* response (*close to zero*). As suggested from this contour plot, stability could be achieved when working in the temperature region of around 4°C to 6°C, and a concentration rate ranging from 1 to 25 at a fixed stirrer time of 150%.

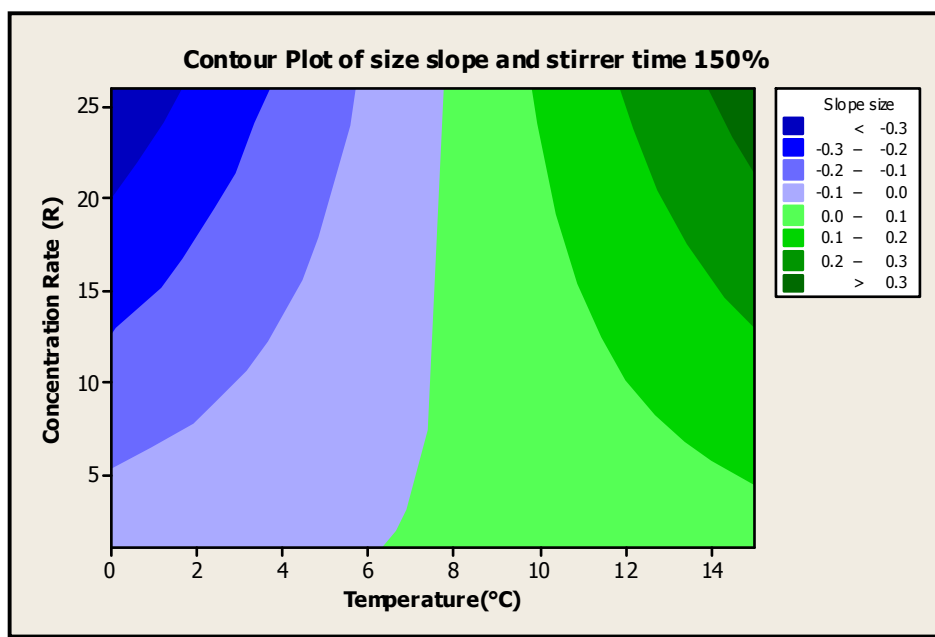


Figure 31. Contour plot for *size slope* at stirrer time 150%

The following figures show the contour plots for *size l* and *size slope* when the temperature was set at 0 °C and 15°C.

Figure 34 shows the region (dark blue area) where small particles could be synthesized. From these results we can suggest, for small particles, to set the synthesis to low concentrations ($R \sim 1$ to 3), with a stirring time ranging from 50 to 150, and a temperature of 0°C.

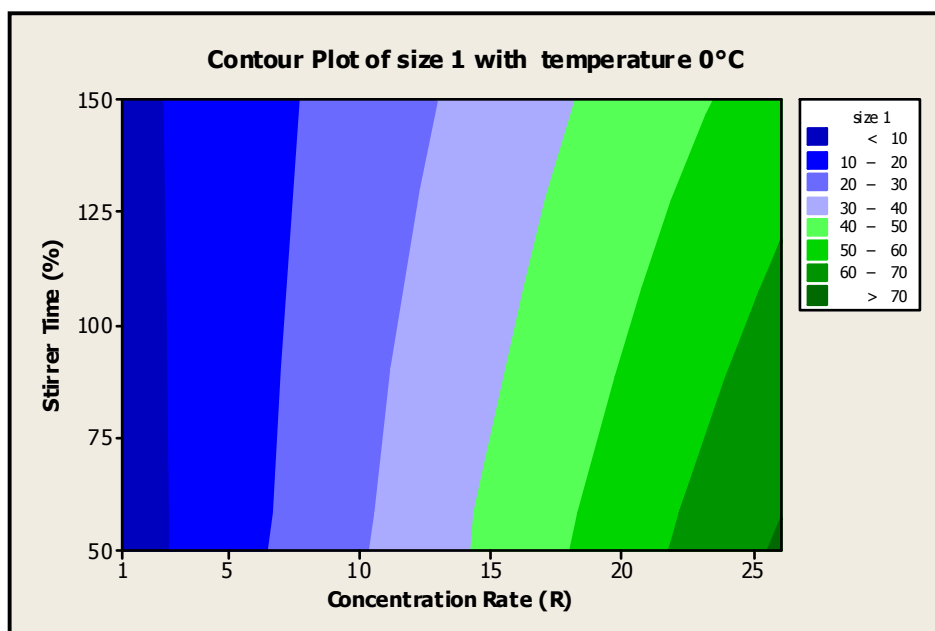


Figure 32. Contour plot for *size 1* at stirrer time 0°C

Figure 33 shows the region (dark green area) where stability is possible by controlling the synthesis parameters. As can be observed, stability is achievable by controlling the concentration rate to the 1 to 5 range while controlling the stirring time to levels ranging from 50% to 75% at a fixed temperature of 0°C. From this graph it is possible to see that the concentration rate has a significant effect in the stability compared with the stirrer factor.

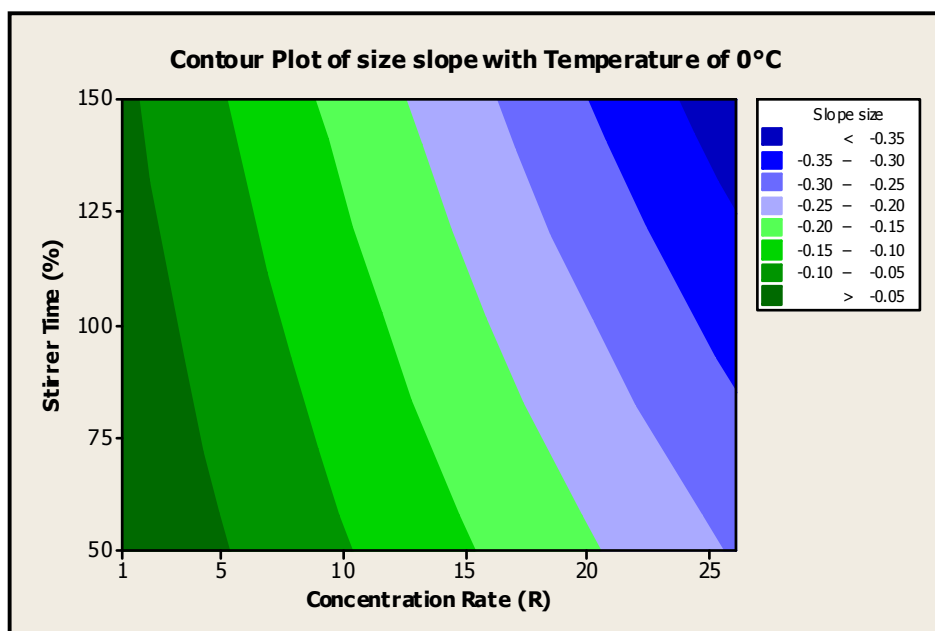


Figure 33. Contour plot for *size slope* and stirrer time 0°C

Figure 34 depicts the experimental region (dark blue area) where it is possible to obtain the smallest particles by controlling the synthesis. In this instance, it is possible to synthesized small particles if the concentration rate is kept to 1 – 3 while stirring from 50 to 150 % as a temperature of 15°C.

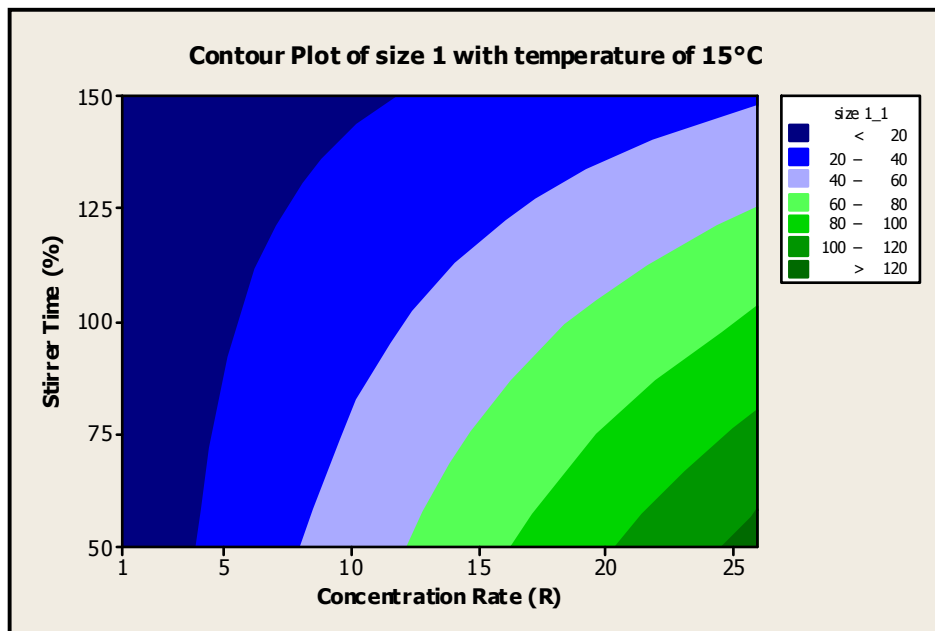


Figure 34. Contour plot for *size 1* at temperature 15°C

Figure 35 presents the region (dark green area) where stability could be obtained for specific experimental conditions. Stability is possible when fixing the temperature to 15°C if the concentration is set to a range of 1 to 25 while stirring the mix from 120 to 150%. From this graph it is also possible to see that the concentration rate has a significant effect in the stability as compared with stirrer time the factor in these conditions.

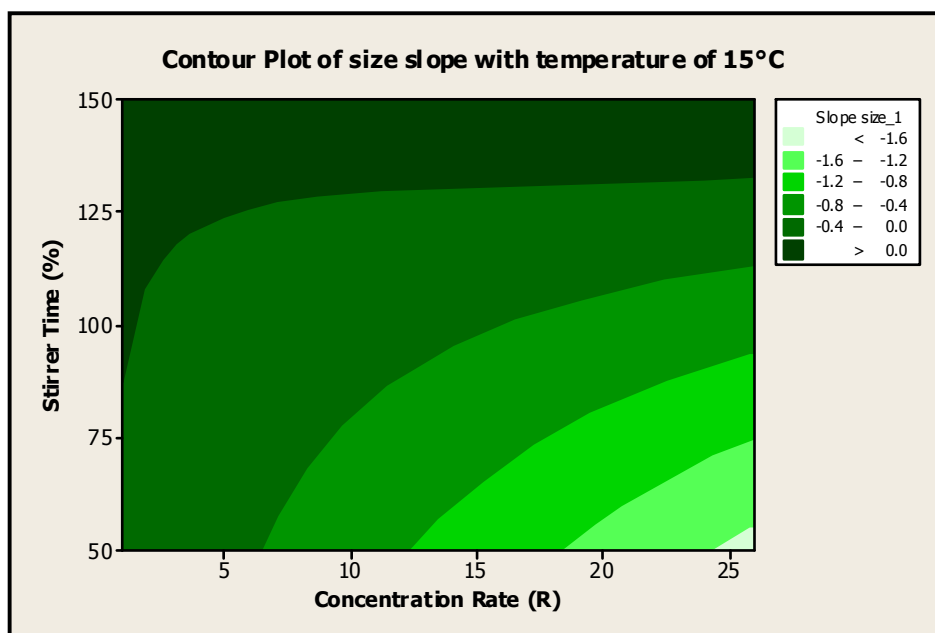


Figure 35. Contour plot for *size slope* at temperature 15°C

The following figures show the contour plots for size 1 and size slope when the concentration of borohydride was set at 1 and 26.

Figure 36 shows the region (gray area) where it is possible to obtain small values for *size 1* (average 5 nm). Low levels of stirrer time (~ 50% to 65%) with low values of temperature (0 °C to 6 °C) are suggested in order to obtain the smallest sizes at a concentration rate of 1. It is possible to see that controlling the stirrer time, the obtained *size 1* values ranged from 5 nm to 7 nm. From the plots it was found that the variation of temperature has not a significant effect on *size 1* values without variation of stirrer time and concentration level at 1.

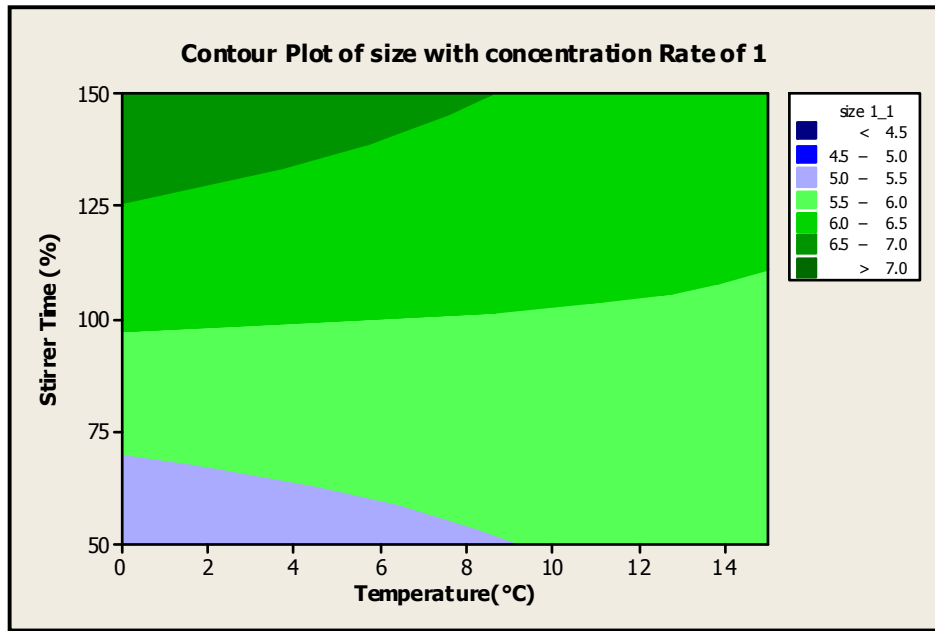


Figure 36. Contour plot for *size 1* at concentration rate of 1

Figure 37 presents the experimental region (gray area) in which stability can be obtained with the proper control of critical synthesis parameters. Low levels of stirrer time (~ 50% to 80%) at temperatures of 0 °C to 7 °C are suggested to obtain values of *size slope* close to zero, if a concentration rate is set at 1. From contour plots it was found that the variation of temperature has not a significant effect on *size slope* as well as the stirrer time variations for concentration rate level of 1.

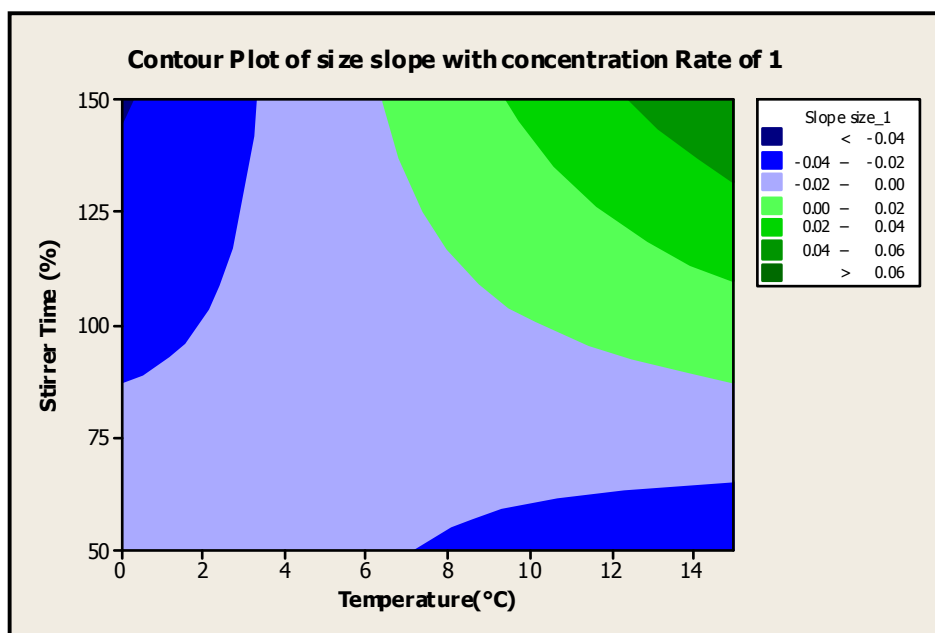


Figure 37. Contour plot for *size slope* at concentration rate of 1

Figure 38 show the region (light green area) where particle sizes ranging from 40 to 60 nm could be obtained if a concentration rate of 26 is used. From our results it was obtained that the sole variation of temperature has no significant effect on particle size if it is not combined with variations of stirrer time and concentration level at 26.

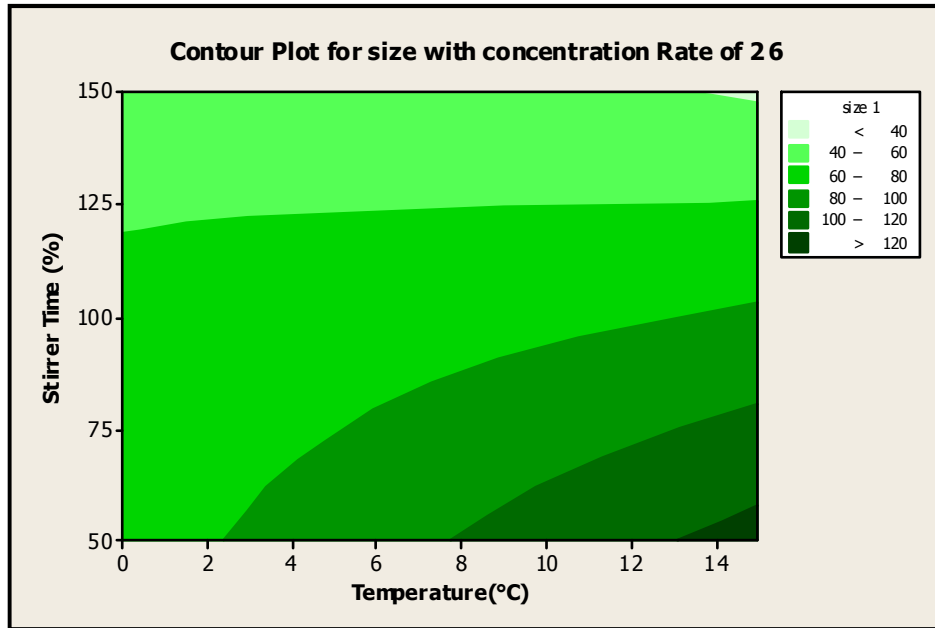


Figure 38. Contour plot for *size 1* at concentration rate of 26

Figure 39 shows the region (dark green area) where stability is achievable by controlling the process.

Low levels of temperature ($\sim 0^{\circ}\text{C}$ to 2°C) did not affect stability for none of the tested stirring times.

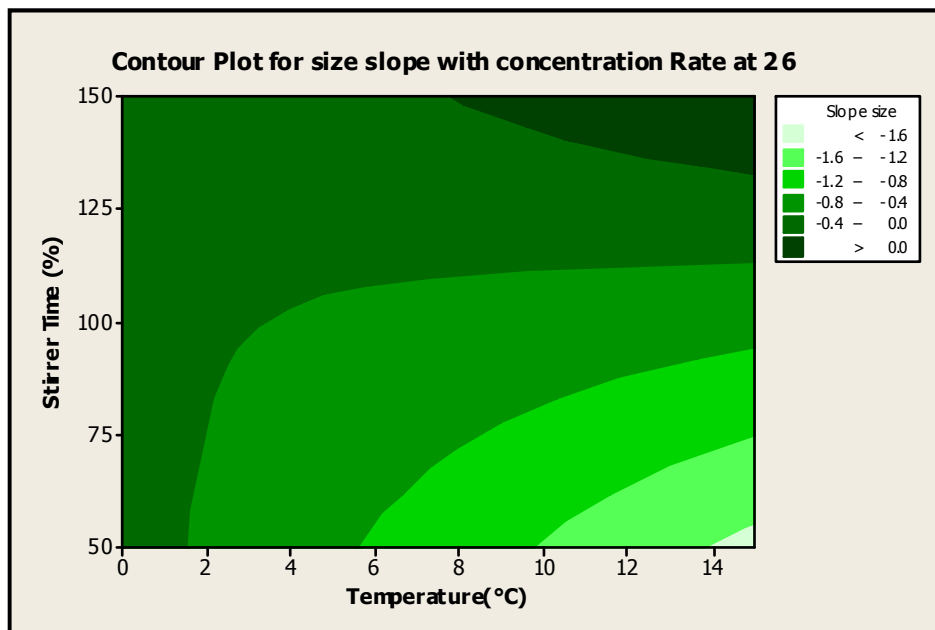


Figure 39. Contour plot for *size slope* at concentration rate of 26

In general, it is concluded that at low concentration rate values we can expect to obtain particles ranging from 5 nm to 20 nm, whereas for high concentrations levels particles will be around 40 nm to 120 nm. When low levels of concentration rate are used, the significant factor controlling particle size was obtained to be the stirrer time instead of the synthesis temperature. However, when high levels of concentration rate are used the temperature dominates the resulting particle size over the stirrer time. For synthesis temperatures ranging from 0°C to 15°C the stirrer time had no significant effect on *size I* and *size slope* values as the concentration rate had. For stirrer times of 50% and 150% the concentration rate had a significant effect on *size I* values whereas temperature did not significantly affect the result. For the stirrer time at 150%, temperature and concentration rate were found to have a significant effect on the colloid stability as measured by the *size slope* response. It is important to note that the effect of temperature was more influenced by the interaction with the concentration rate than with the stirrer time. A reduction of the concentration level is suggested in order to better define the effect of temperature on

the synthesis. The interaction of stirrer time and concentration rate factor was pivotal in controlling particle size, whereas the interaction of stirrer time and temperature was crucial in controlling colloid stability. With this information we can confirm that the three factors are significant in the synthesis of silver NP's.

6.5.3 Center points

The center points in this design of experiments structure can be used to test if the response is a linear function of the input variables (factors) between high and low settings .If the difference between average values of corner and center points is significant (lower o higher), then there exist a second order model [13]. If the response is not linear, additional runs may be added to the original experiment allowing to model this curvature with a second-order model [29]. In this work, the average values of the corner points for *size 1*, *size 2* and *size slope* were 39.39 nm, 21.13 nm and -0.25 respectively, and the average values of the center points for the same responses were 27.86 nm, 3.34 nm and -0.34. It is possible to see that the difference is not large enough between the responses for corner and center points, just for the response of *size 1* there exists a difference of roughly 10 nm (less than the standard deviation) which indicates that there is not a significant difference between these values. From these results it was concluded that there is not curvature in these three response surface. This conclusion was determined from using the value of deviation standard selected in section 5.1 which was roughly of 18 nm.

From the statistical model it is possible to define the optimal process parameters in this case, so that the stability can be controlled. By controlling all these factors a feasible area for stability can be obtained. As future work we recommend the implementation of the modeled process settings so that the results can be validated and further optimization can be performed.

6.6 Results from the combinations from design of experiments

Sample M11550 showed a notable change in the color for the Ag colloid (Figure 42 to Figure 45), it changed from shiny yellow to brown yellow. In the UV- vis graphs (see Figure 81 to Figure 82) it was possible to observe an increment in the peak width from time 1 to time 2, where a blue shift occurred from 495 nm to 490 nm. Sample M10150 also presented a significant change in the color of the Ag colloid (Figure 46 to Figure 50), shifting from a concentrated shiny yellow to a brown yellow. In the UV- vis graphs (Figure 83 and Figure 84) it was found that the plasmon was kept in 495 nm for time 1 and time 2. Sample M1050 did not present significant color change between time 1 and time 2 (Figure 51 to Figure 54), the color changed only for the replicates , one replicate was shine yellow and this color was kept for time 2, and the other was brown yellow and this color was kept for time 2. A precipitated effect was expected based on the settings of stirrer time (50%), however did not occurred. Sample M12575100 showed significant change in color for Ag colloid (Figure 55 to Figure 60), it changed from concentrated shiny yellow to a dark brown . A precipitated effect not was expected due the level of stirrer time (100%). For the UV- vis graphs (Figure 85 and Figure 86) a plasmon change was observed from 495 to 485 nm for time 1 and time 2, respectively. There was a notable increase in the width for the absorbance peak for this sample from time 1 to time 2.

Sample M2615150 presented a notable change in color for the Ag colloid (Figure 67 to Figure 72), it changed from a shiny yellow to a dark brown. Precipitation occurred as expected.

Owing to the fact that stirrer time was set to 150%. From the UV- vis graphs (Figure 89 and Figure 90) an increment of the peak width from time 1 to time 2 was observed with together with a blue shift from 495 nm to 487 nm. This sample presented a significant change in the wide of the peak. The sample M261550 presented a significant change in the color in the Ag colloid (Figure 73 to Figure 78), the color changed from shine yellow to dark brown. A precipitated effect was expected due the level of stirrer time

(50%). In the UV- vis graphs (Figure 91 and Figure 92) it was possible to note that the Plasmon changed from 490 nm to 485 nm . The sample 260150 presented a notable change in the color in the Ag colloid (Figure 61 to Figure 66), the color changed from shine yellow to dark brown. A precipitated effect was expected due the level of stirrer time (150%), however it not occurred. In the UV- vis graphs (Figure 87 and Figure 88) it was possible to note that the Plasmon changed from 492 nm to 487 nm . For the sample M26050 presented a significant change in the color in the Ag colloid (Figure 79 to Figure 80), the color changed from shine yellow to dark brown . A precipitated effect not was expected due the level of stirrer time (50%). In the UV- vis graphs (see Figure 93 and Figure 94) it was possible to note that the Plasmon changed from 492 to 485 nm for time 1 and time 2, respectively. There was a notable increase in the wide and reduction of high in the absorbance peak for this sample from time 1 to time 2.

6.7 Discussion of the effect for the concentration rate, temperature and stirrer time on the stability of Ag colloid

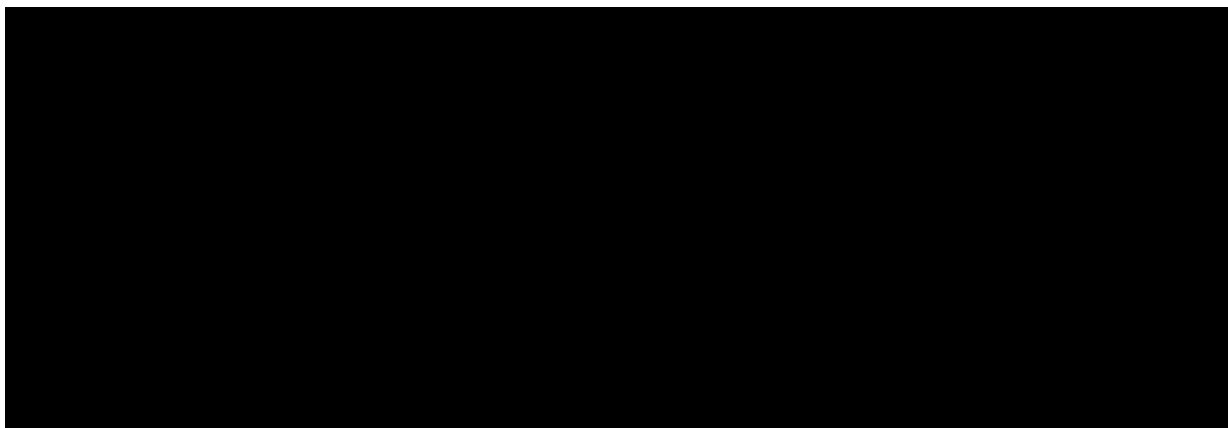
As observed from our results, smaller sizes obtained were found at low concentration rates of sodium borohydride, whereas the larger particle sizes were obtained at high concentration levels of this factor.

Our synthesis process the borohydride had multiple functions: it reduced the silver salt, it was partially consumed in the hydrolysis process, and also provided a capping effect around the nanoparticles by an electrostatic effect. Most of the samples at high concentration showed dark colors at time 2. For high levels, due the over ionic strength value, the agglomeration was expected as explained in chapter 2. The stirrer time was important factor to keep the homogeneity of the NP's colloid, thus avoiding the early agglomeration and enhancing the homogeneous distribution of borohydride anions. From our work it was shown that this control was not possible to obtain when low and high concentrations of reducer agent were used. The precipitated was observed in the solutions where the stirrer time (%) is less or bigger than the synthesis time, i.e. , the time required to add all the silver nitrate solution into the sodium borohydride solution.

The temperature was found to be pivotal in controlling the nucleation growth of the NP's, as well of the hydrolysis of borohydride anions. In low temperatures the hydrolysis of borohydride takes low rate, also, is known that in low temperatures values the hydrolysis of sodium borohydride occurs at slow rate.

The pH value of the solution had an important roll in keeping the stability on the system as given by the small values of the *size slope*. After the reduction of the silver salt, the borohydride anion is converted to borane ions whit a weak acidic pH. Then when an excess of sodium borohydride is used a hydrolysis start yielding borates ions which are strongly basic. The basic pH stops the hydrolysis process allowing the borohydride anion to provide nanoparticle stability. The pH values ranging from 4 to 7.5 are known to act against the stability of the Ag colloid systems [11]. Therefore pH values of 8 or higher are desired when stability is needed. Table 5 shows pH values for the samples synthesized throughout this work.

Table 5. pH values for the synthesized samples



6.8 The best synthesis condition (combination)

From our experimental trials it was found that the best embodiment of the synthesis which resulted in a small particle size as well as acceptable stability corresponded to the center point (M-12.5 7.5 100). Thus showing that with 100% stirrer time and 12.5 of concentration stability sizes are possible. This combination resulted in a small *size slope* (-0.34).

7 Conclusions

Silver NP's have been successfully synthesized in DI water using sodium borohydride as reducer agent by oxide reduction method. When low concentration rates (R) of sodium borohydride were used the full amount of silver nitrate was not reduced, whereas when a high concentration of sodium borohydride was used agglomeration of the nanoparticles occurred due the overall ionic strength. It was found that for all samples with R=26 the color of the colloid changed from shiny yellow to dark yellow or brown, such effect, indicated that the agglomeration was occurred. With low concentrations of sodium borohydride (R=1) the yellow color of the colloid was held. A blue shift effect from the UV-vis results suggested a microfloculation effect on the nanoparticles which is indicative of instability of the system. Low synthesis temperatures proved to be critical for obtaining small particle sizes. The ANOVA results from our DOE showed that the interaction between stirrer time, temperature, and sodium borohydride concentration have a significant effect in the synthesis process of the Ag NP's. With these results we can claim that the particle size and the stability of the colloid is possible by the proper control of the synthesis parameters, which was the main objective of our work. The developed statistical model allows the practitioner to predict colloidal stability and size by controlling synthesis parameters. The best combination was obtained in sample M12.57.5100, which resulted in a small size (time 1: 27.88 nm and time 2: 3.34 nm) and small values for *size slope* (-0.34).

8 REFERENCES

- [1] R. Kisiel y Z. Szczepański, «Die-attachment solutions for SiC power devices», *Microelectronics Reliability*, vol. 49, n.º. 6, pp. 627–629, jun. 2009.
- [2] H. Masuo, N. Kiyoshi, y N. Makio, *Nanoparticle Technology Handbook*, First. Elsevier, 2007.
- [3] James E Morris, *Nanopackaging: Nanotechnologies end electronic packaging*, First. Springer, 2008.
- [4] H. Jiang, K. Moon, F. Hua, y C. P. Wong, «Synthesis and Thermal and Wetting Properties of Tin/Silver Alloy Nanoparticles for Low Melting Point Lead-Free Solders», *Chem. Mater.*, vol. 19, n.º. 18, pp. 4482–4485, ago. 2007.
- [5] F. Hua,, H. Dong,, y K. Moon,, «Thermal Properties of Oxide Free Nano Non Noble Metal for Low Temperature Interconnect Technology,», presented at the Proceedings of the 56th IEEE Electronic Components and Technology Conference, San Diego, CA,, 2006.
- [6] P. Quintero, T. Oberc, y P. McCluskey, «Reliability assessment of high temperature lead-free device attach technologies», 2008.
- [7] M. Rycenga, C. M. Cobley, J. Zeng, W. Li, C. H. Moran, Q. Zhang, D. Qin, y Y. Xia, «Controlling the Synthesis and Assembly of Silver Nanostructures for Plasmonic Applications», *Chem. Rev.*, vol. 111, n.º. 6, pp. 3669–3712, mar. 2011.
- [8] J. Chang, J. H. Lee, J.-H. Cha, D.-Y. Jung, G. Choi, y G. Kim, «Bimetallic nanoparticles of copper and indium by borohydride reduction», *Thin Solid Films*, vol. 519, n.º. 7, pp. 2176–2180, ene. 2011.
- [9] A. Panáček, L. Kvítek, R. Prucek, M. Kolář, R. Večeřová, N. Pizúrová, V. K. Sharma, T. Nevěčná, y R. Zbořil, «Silver Colloid Nanoparticles: Synthesis, Characterization, and Their Antibacterial Activity», *J. Phys. Chem. B*, vol. 110, n.º. 33, pp. 16248–16253, 2006.
- [10] H. S. C., *Colloidal phenomena : advanced topics*. Noyes Publications, 1985.
- [11] Malvern Instruments, «Zeta Potential An Introduction in 30 Minutes». 2004.
- [12] Malrvern Instruments, «Zeta Sizer Nano Series User Manual». 2004.
- [13] *Montgomery D. Design and Analysis of experiments. 7th ed. John Wiley and Sons Inc.; 2008. .*
- [14] L. Mulfinger, S. D. Solomon, M. Bahadory, A. V. Jeyarajasingam, S. A. Rutkowsky, y C. Boritz, «Synthesis and Study of Silver Nanoparticles», *J. Chem. Educ.*, vol. 84, n.º. 2, p. 322, 2007.
- [15] X. Dong, X. Ji, H. Wu, L. Zhao, J. Li, y W. Yang, «Shape Control of Silver Nanoparticles by Stepwise Citrate Reduction», *J. Phys. Chem. C*, vol. 113, n.º. 16, pp. 6573–6576, 2009.
- [16] X. Song, S. Sun, W. Zhang, y Z. Yin, «A method for the synthesis of spherical copper nanoparticles in the organic phase», *Journal of Colloid and Interface Science*, vol. 273, n.º. 2, pp. 463–469, may 2004.
- [17] S. S. Mansouri y S. Ghader, «Experimental study on effect of different parameters on size and shape of triangular silver nanoparticles prepared by a simple and rapid method in aqueous solution», *Arabian Journal of Chemistry*, vol. 2, n.º. 1, pp. 47–53, jul. 2009.
- [18] «Synthesis of silver nanorods and application for die attach material in devices», *J. Matter Sci: Mater Electron*, vol. 21, pp. 713–718, 2010.
- [19] A. Zielińska, E. Skwarek, A. Zaleska, M. Gazda, y J. Hupka, «Preparation of silver nanoparticles with controlled particle size», *Procedia Chemistry*, vol. 1, n.º. 2, pp. 1560–1566, nov. 2009.

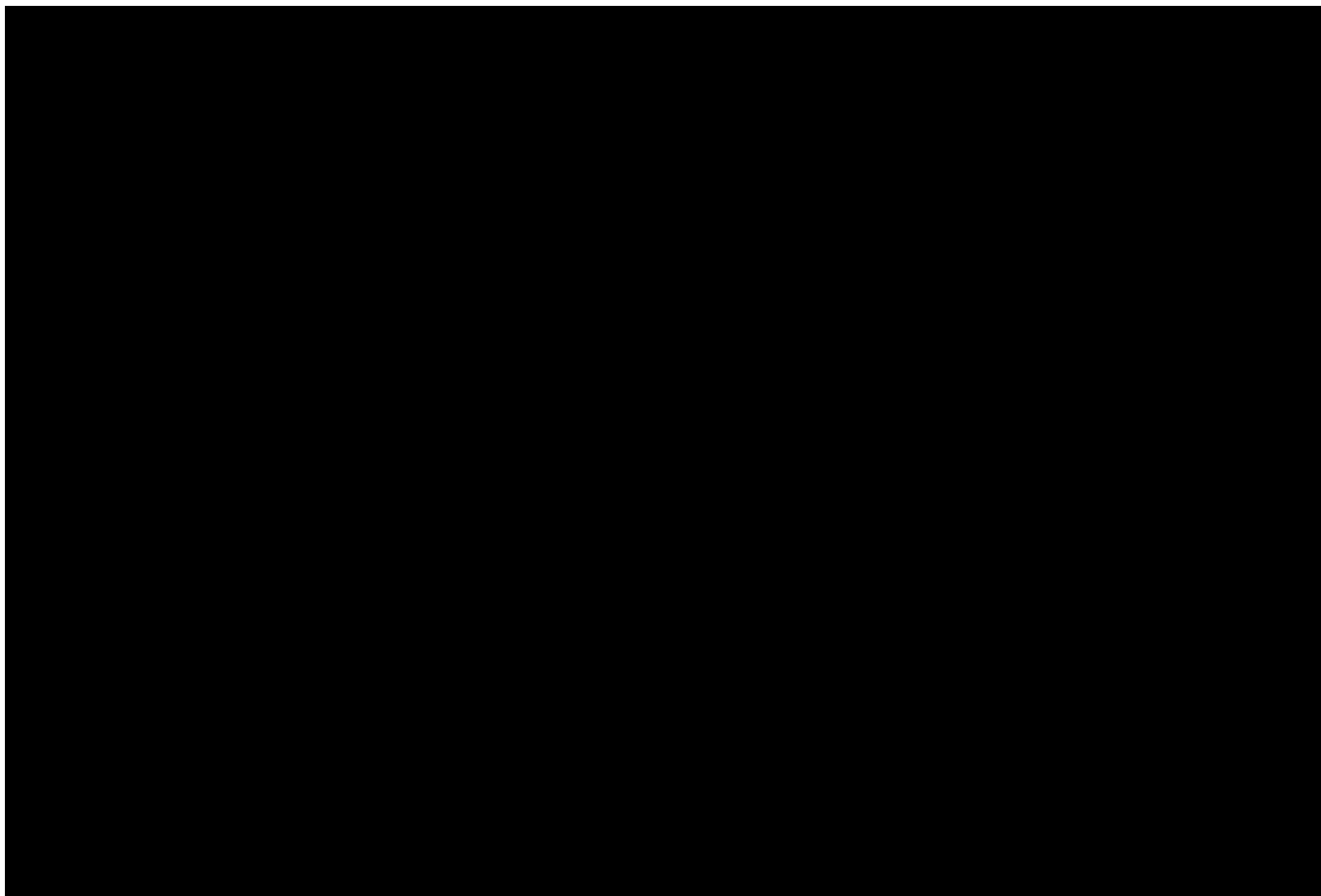
- [20] E. Bulut y M. Özacar, «Rapid, Facile Synthesis of Silver Nanostructure Using Hydrolyzable Tannin», *Ind. Eng. Chem. Res.*, vol. 48, n°. 12, pp. 5686–5690, may 2009.
- [21] D. L. Van Hying y C. F. Zukoski, «Formation Mechanisms and Aggregation Behavior of Borohydride Reduced Silver Particles», *Langmuir*, vol. 14, n°. 24, pp. 7034–7046, 1998.
- [22] David D. Evanoff Jr. y George Chumanov, «Synthesis and Optical Properties of Silver Nanoparticles and Arrays», vol. 6, pp. 1221 – 1231, 2005.
- [23] Z. Khan, J. I. Hussain, S. Kumar, y A. A. Hashmi, «Silver nanoplates and nanowires by a simple chemical reduction method», *Colloids and Surfaces B: Biointerfaces*, vol. 86, n°. 1, pp. 87–92, ago. 2011.
- [24] T. Dadosh, «Synthesis of uniform silver nanoparticles with a controllable size», *Materials Letters*, vol. 63, n°. 26, pp. 2236–2238, oct. 2009.
- [25] J. Liu, X. Li, y X. Zeng, «Silver nanoparticles prepared by chemical reduction-protection method, and their application in electrically conductive silver nanopaste», *Journal of Alloys and Compounds*, vol. 494, n°. 1–2, pp. 84–87, 2010.
- [26] X. Dong, X. Ji, J. Jing, M. Li, J. Li, y W. Yang, «Synthesis of Triangular Silver Nanoprisms by Stepwise Reduction of Sodium Borohydride and Trisodium Citrate», *J. Phys. Chem. C*, vol. 114, n°. 5, pp. 2070–2074, 2010.
- [27] Rotello, Vincent M., *Nanoparticles: building blocks for nanotechnology*. Series Editor: David J Lookwood, 2004.
- [28] K.-S. Chou, Y.-C. Chang, y L.-H. Chiu, «Studies on the Continuous Precipitation of Silver Nanoparticles», *Ind. Eng. Chem. Res.*, vol. 51, n°. 13, pp. 4905–4910, mar. 2012.
- [29] L. J. Kirk McNeilly, «Results May Not vary», *www.qualityprogress.com*, pp. 42–48, may 2011.
- [30] Y. Cedeño-Mattei, O. Perales-Perez, M. Sánchez-Peña, y M. Cabrera-Ríos, «Experimental Optimization of Nanomagnetic Properties», presented at the Proceedings of the 2009 Industrial Engineering Research Conference., Miami, FL, USA, 2009.
- [31] D. L. Van Hying, W. G. Klemperer, y C. F. Zukoski, «Characterization of Colloidal Stability during Precipitation Reactions», *Langmuir*, vol. 17, n°. 11, pp. 3120–3127, may 2001.
- [32] J. Wagner, T. R. Tshikhudo, y J. M. Köhler, «Microfluidic generation of metal nanoparticles by borohydride reduction», *Chemical Engineering Journal*, vol. 135, Supplement 1, n°. 0, pp. S104–S109, ene. 2008.
- [33] Van Vlack, Lawrence H., *Elements of materials science and engineering*, Sixth Edition. 1989.
- [34] Ham, Frank S., «Diffusion-Limited Growth of Precipitate Particles», *Journal of Applied Physics*, vol. 30, n°. 10, pp. 1518 – 1525, 1959.
- [35] Kotz, *Chemistry & chemical reactivity*. Seventh Edition, 2009.
- [36] Jack Bonsak, «Thesis: Chemical synthesis of silver nanoparticles for light trapping applications in silicon solar cells», University of Oslo, 2010.
- [37] Duncan J Shaw, *Introduction to colloid and Surface Chemistry*, Third Edition. 1989.
- [38] E. G. Larissa V. Stebounova, *Silver nanoparticles in simulated biological media: a study of aggregation, sedimentation, and dissolution*. J Nanopart Res, 2011.
- [39] Malvern Instruments, «Derjaguin, Landau, Verwey and Overbeek theory». Malvern Instruments.http://www.malvern.com/labeng/industry/colloids/dlvo_theory.htm.

- [40] Dr. Kishor Wasan Laboratory, «Flocculation and deflocculation». Division of Pharmaceutics and Biopharmaceutics Faculty of Pharmaceutical Sciences University of British Columbia. <http://www.wasanlab.com/pharm/flocc.html>.
- [41] H. I. Schlesinger, Herbert C. Brown, A. E. Finholt, James R. Gilbreath, Henry R. Hoekstra, and Earl K., *Sodium Borohydride, Its Hydrolysis and its Use as a Reducing Agent and in the Generation of Hydrogen*. Hyde Journal of the American Chemical Society 1953.
- [42] R. Leardi, «Experimental design in chemistry: A tutorial», *Analytica Chimica Acta*, vol. 652, n°. 1–2, pp. 161–172, oct. 2009.
- [43] C. Manterola y V. Pineda, «El valor de “p” y la “significación estadística”. Aspectos generales y su valor en la práctica clínica*», *Rev. Chilena de Cirugía*, vol. 60, n°. 1, pp. 86–89, feb. 2008.
- [44] M. Molina y Pedro Quintero, «Thesis: Structural transformations of low temperature, pressureless sintered silver nanoparticles for die attach interconnections», 2012.
- [45] Malvern Instruments, «A basic guide to particle characterization». Malvern Instruments, 2012.
- [46] B.D. Cullity, *Elements of X-ray diffraction*, Third edition. Prentice Hall, 2001.
- [47] S. Z. Lin Li, Ashok Kumar, *Materials characterization techniques*". CRC Press, 2009.
- [48] A. J. Frank, N. Cathcart, K. E. Maly, y V. Kitaev, «Synthesis of Silver Nanoprisms with Variable Size and Investigation of Their Optical Properties: A First-Year Undergraduate Experiment Exploring Plasmonic Nanoparticles», *J. Chem. Educ.*, vol. 87, n°. 10, pp. 1098–1101, jun. 2010.
- [49] Z. Khan, S. A. Al-Thabaiti, E. H. El-Mossalamy, y A. Y. Obaid, «Studies on the kinetics of growth of silver nanoparticles in different surfactant solutions», *Colloids and Surfaces B: Biointerfaces*, vol. 73, n°. 2, pp. 284–288, 2009.
- [50] Y. Xia y D. J. Campbell, «Plasmons: Why Should We Care?», *J. Chem. Educ.*, vol. 84, n°. 1, p. 91, ene. 2007.

APPENDIX A

Factors of experimentation

Table 6. Chemical amounts used in the experiment



9 APPENDIX B

Interval plot Results cont.

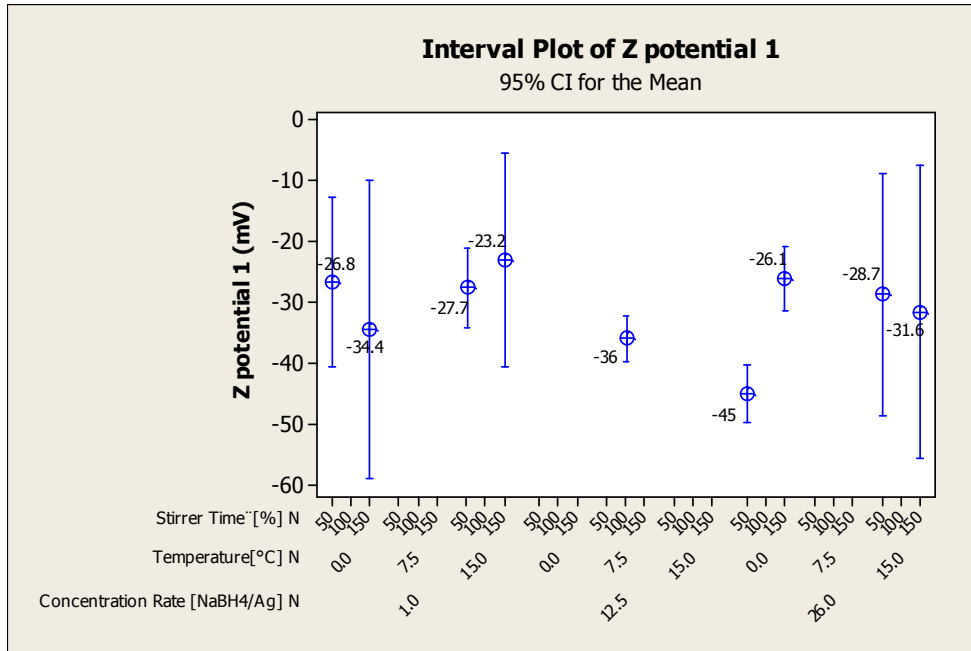


Figure 40. Interval plot of Z potential 1

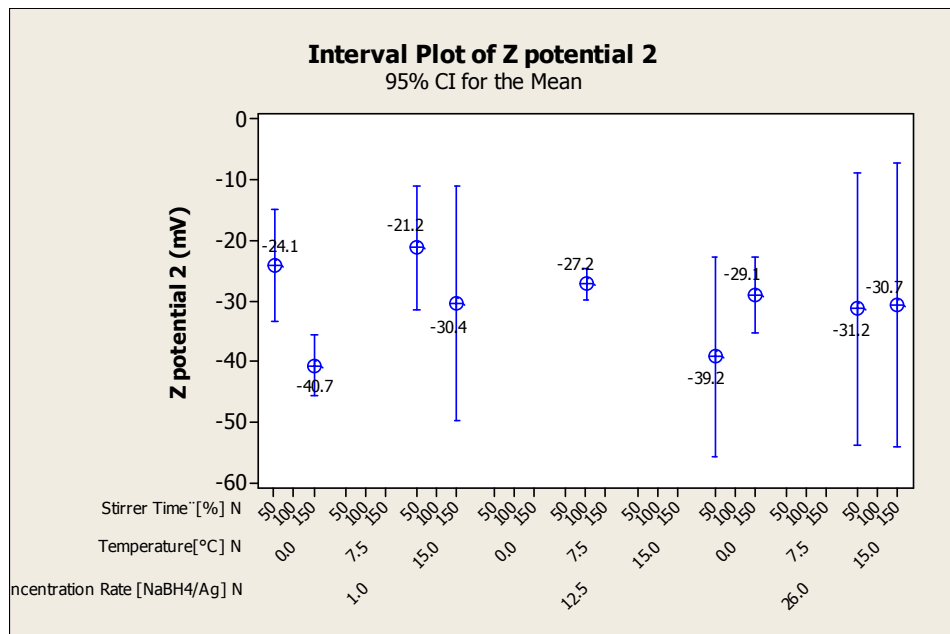


Figure 41. Interval plot for Z potential 2

10 APPENDIX C

The following images show the colors for the combinations of colloids.

a) 	
Figure 42. Color of colloid for combination M1-11550 in time 1	Figure 43. Color of colloid for combination M1-11550 in time 2

b) 	
Figure 44. Color of colloid for combination M2-11550 in time 1	Figure 45. Color of colloid for combination M2-11550 in time 2

a)		
<p>Figure 46. Color of colloid for combination M1-10150 in time 1</p>		

b)		
<p>Figure 47. Color of colloid for combination M2-10150 in time 1</p>		<p>Figure 48. Color of colloid for combination M2-10150 in time 2</p>

c)		
<p>Figure 49. Color of colloid for combination M3-10150 in time 1</p>		<p>Figure 50. Color of colloid for combination M3-10150 in time 2</p>

	
<p>Figure 51. Color of colloid for combination M1-1050 in time 1</p>	<p>Figure 52. Color of colloid for combination M1-1050 in time 2</p>

	
<p>Figure 53. Color of colloid for combination M2-1050 in time 1</p>	<p>Figure 54. Color of colloid for combination M2-1M1050 in time 2</p>

<p>a)</p> 	
<p>Figure 55. Color of colloid for combination M1-12 5 75 100 in time 1</p>	<p>Figure 56. Color of colloid for combination M1-12 5 75 100 in time 2</p>

<p>b)</p> 	
<p>Figure 57. Color of colloid for combination M2-12 5 75 100 in time 1</p>	<p>Figure 58. Color of colloid for combination M2-12 5 75 100 in time 2</p>

<p>c)</p> 	
<p>Figure 59. Color of colloid for combination M3-12 5 75 100 in time 1</p>	<p>Figure 60. Color of colloid for combination M3-12 5 75 100 in time 2</p>

<p>a)</p> 	
<p>Figure 61. Color of colloid for combination M1-260150 in time 1</p>	<p>Figure 62. Color of colloid for combination M1-260150 in time 2</p>

<p>b)</p> 	
<p>Figure 63. Color of colloid for combination M2-260150 in time 1</p>	<p>Figure 64. Color of colloid for combination M2-260150 in time 2</p>

<p>c)</p> 	
<p>Figure 65. Color of colloid for combination M3-260150 in time 1</p>	<p>Figure 66. Color of colloid for combination M3-260150 in time 2</p>

<p>a)</p> 	
<p>Figure 67. Color of colloid for combination M1-2615150 in time 1</p>	<p>Figure 68. Color of colloid for combination M1-2615150 in time 2</p>

<p>b)</p> 	
<p>Figure 69. Color of colloid for combination M2-2615150 in time 1</p>	<p>Figure 70. Color of colloid for combination M2-2615150 in time 2</p>

<p>c)</p> 	
<p>Figure 71. Color of colloid for combination M2-2615150 in time 1</p>	<p>Figure 72. Color of colloid for combination M2-2615150 in time 2</p>

<p>a)</p> 	
<p>Figure 75. Color of M1-261550 colloid for combination in time 1</p>	<p>Figure 76. Color of colloid of M1-261550 for combination in time 2</p>

<p>b)</p> 	
<p>Figure 73. Color of colloid for combination M2-261550 in time 1</p>	<p>Figure 74. Color of colloid for combination M2-261550 in time 2</p>

<p>c)</p> 	
<p>Figure 77. Color of colloid for combination M3-261550 in time 1</p>	<p>Figure 78. Color of colloid for combination M3-261550 in time 2</p>

<p>a)</p> 	
<p>Figure 79. Color of colloid for combination M1-26050 in time 1</p>	<p>Figure 80. Color of colloid for combination M1-26050 in time 2</p>

11 APPENDIX D

UV vis Results

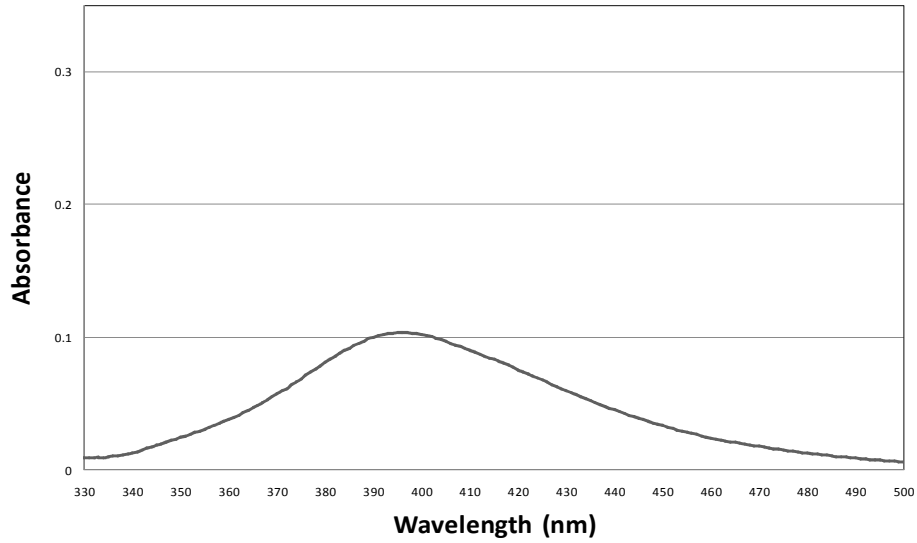


Figure 81. This graph shows the UV vis spectroscopy for the sample M1-11550 in time 1

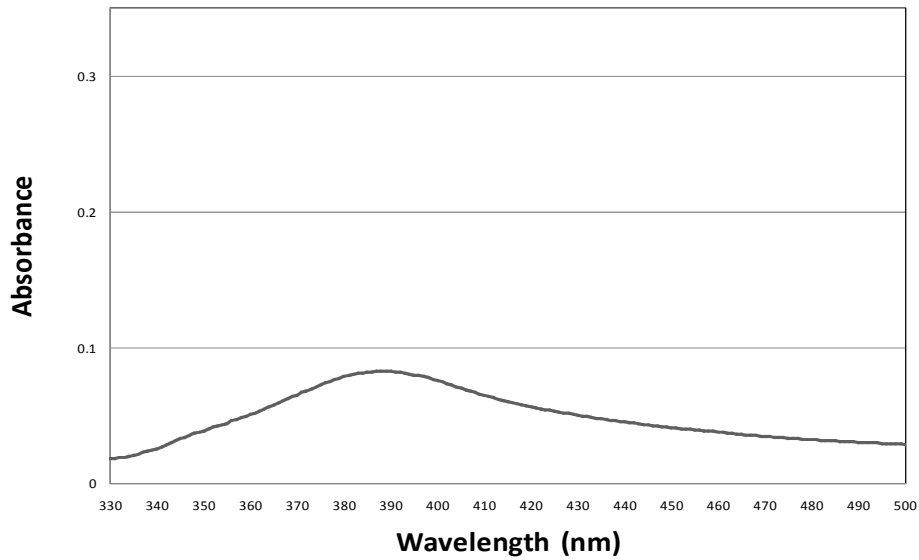


Figure 82. This graph shows the UV vis spectroscopy for the sample M1-11550 in time 2

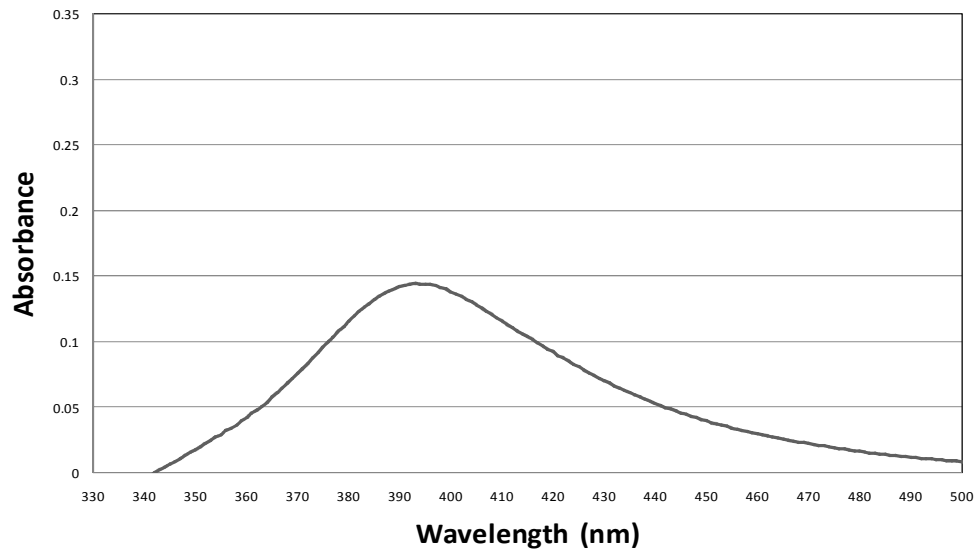


Figure 83. This graph shows the UV vis spectroscopy for the sample M1-10150 in time 1

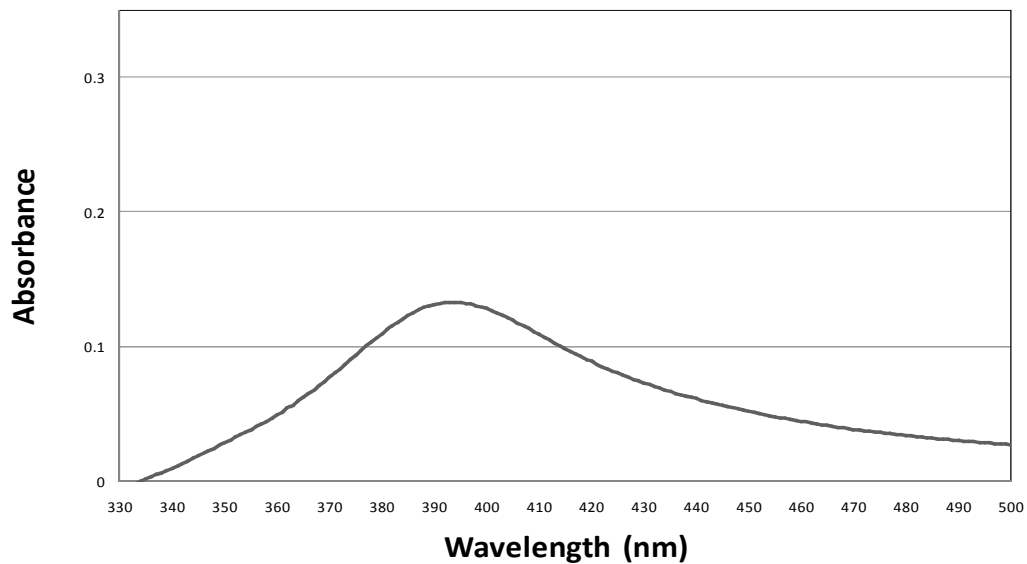


Figure 84. This graph shows the UV vis spectroscopy for the sample M1-10150 in time 2.

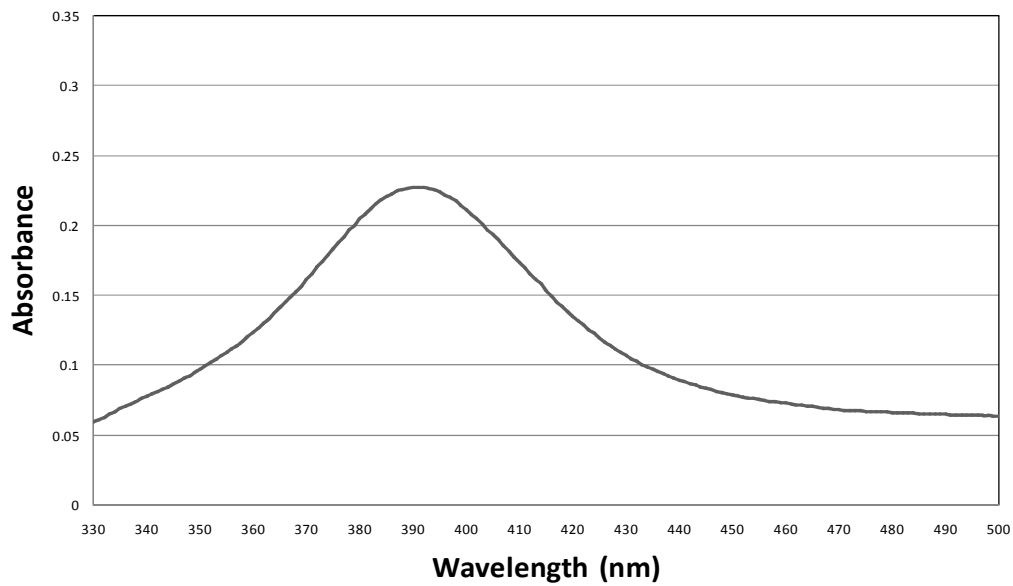


Figure 85. This graph shows the UV vis spectroscopy for the sample M1-12575100 in time 1

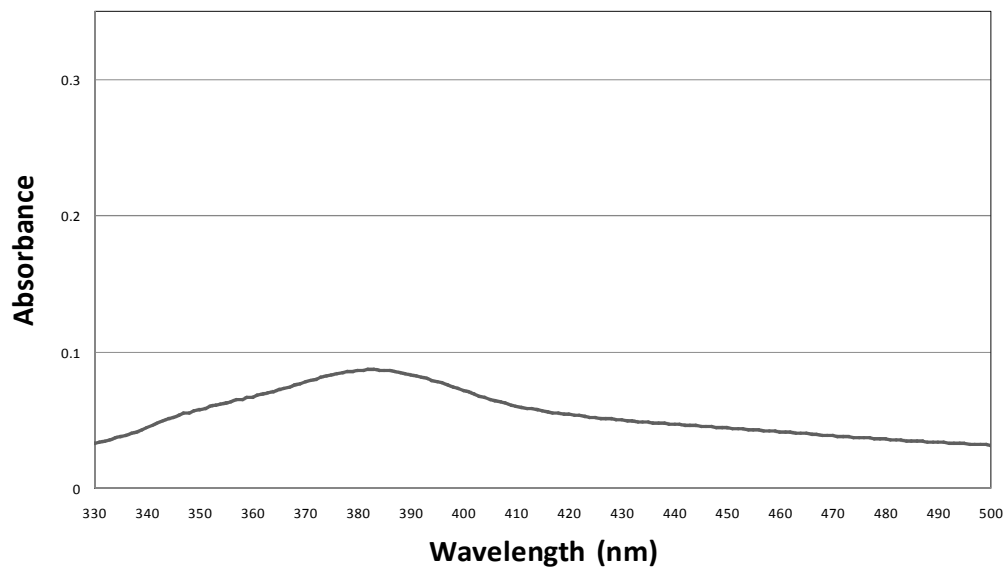


Figure 86. This graph shows the UV vis spectroscopy for the sample M1-12575100 in time 2

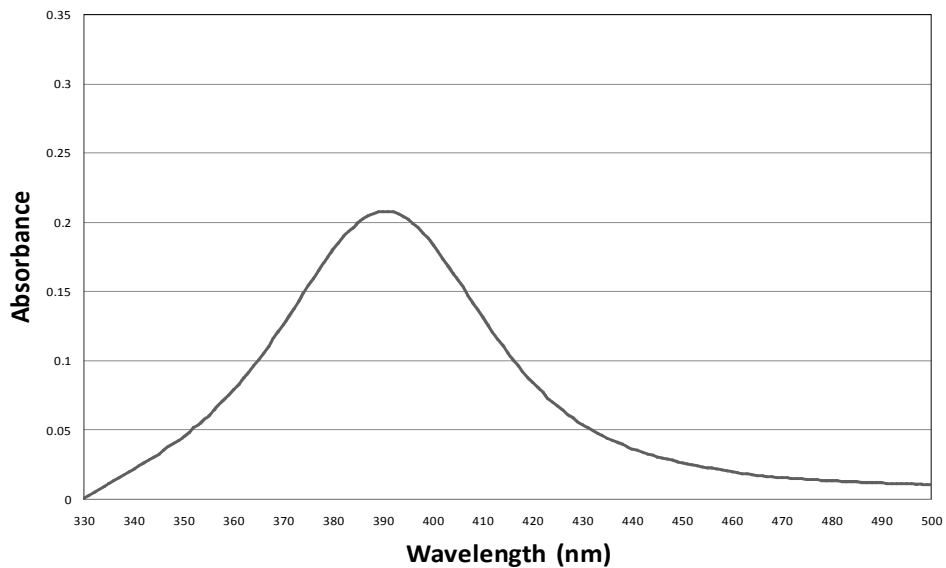


Figure 87. This graph shows the UV vis spectroscopy for the sample M1-260150 in time 1

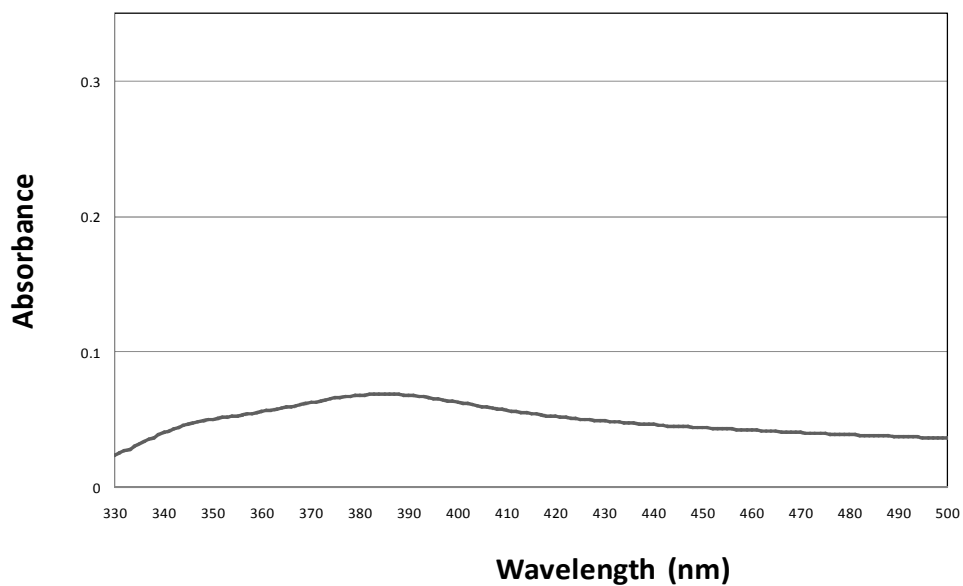


Figure 88. This graph shows the UV vis spectroscopy for the sample M1-260150 in time 2

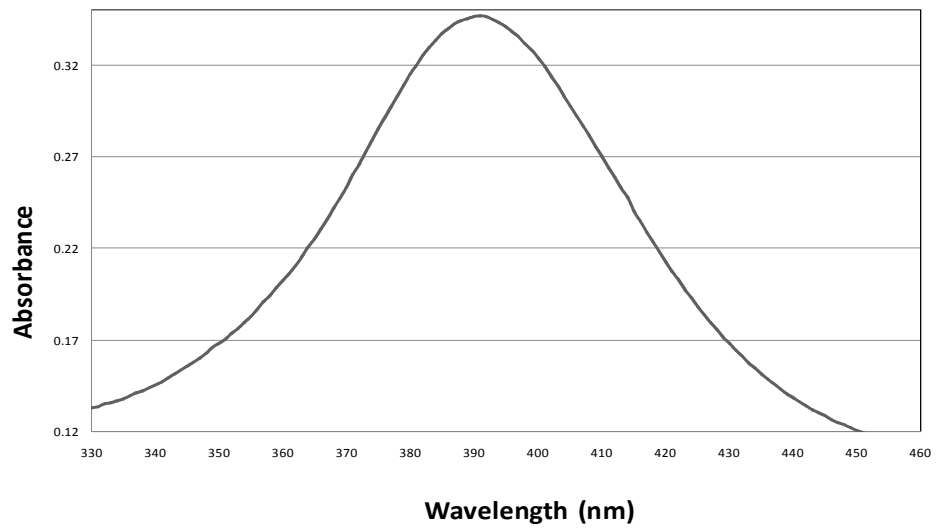


Figure 89. This graph shows the UV vis spectroscopy for the sample M1-2615150 in time 1

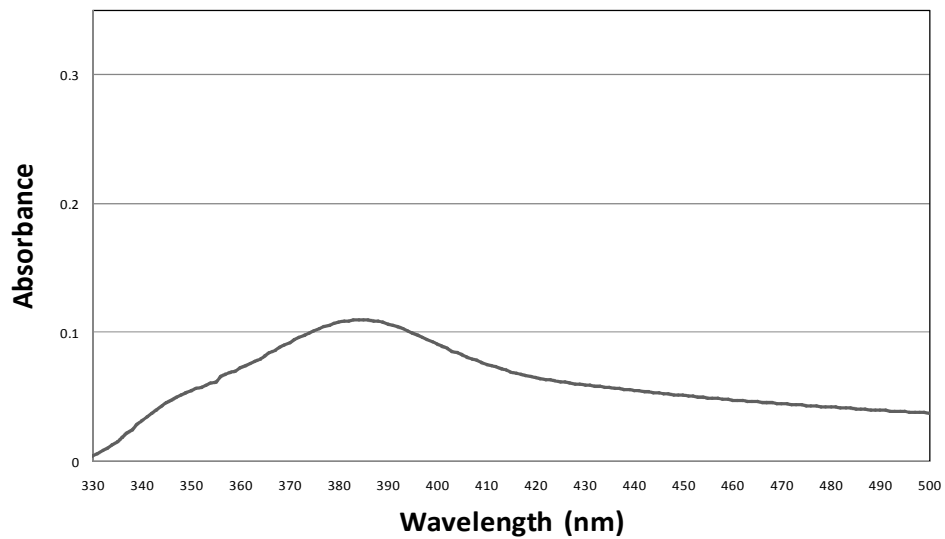


Figure 90. This graph shows the UV vis spectroscopy for the sample M1-2615150 in time 2

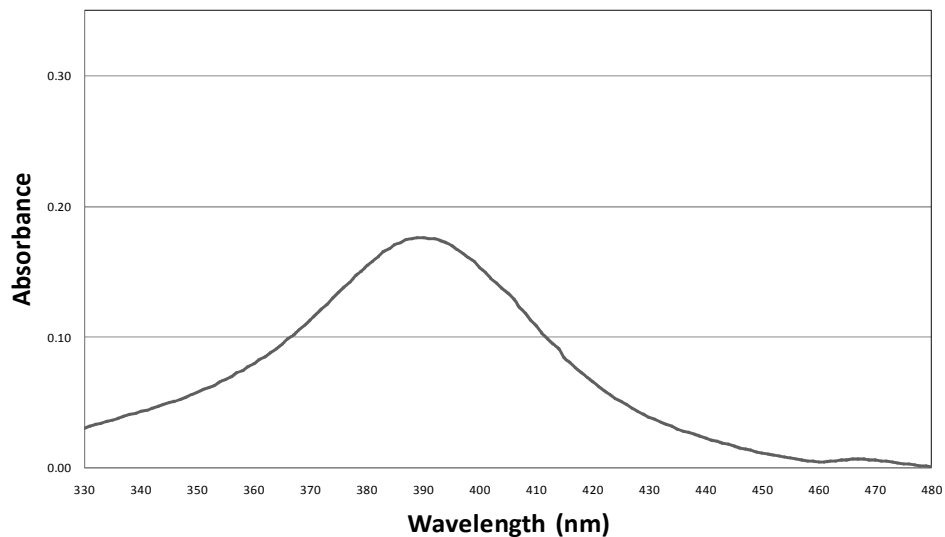


Figure 91. This graph shows the UV vis spectroscopy for the sample M1-261550 in time 1

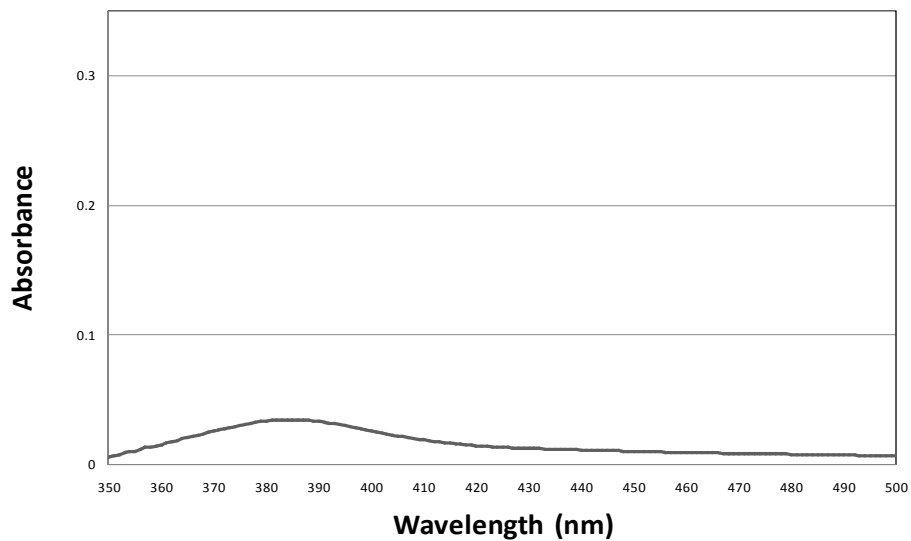


Figure 92. This graph shows the UV vis spectroscopy for the sample M1-261550 in time 2

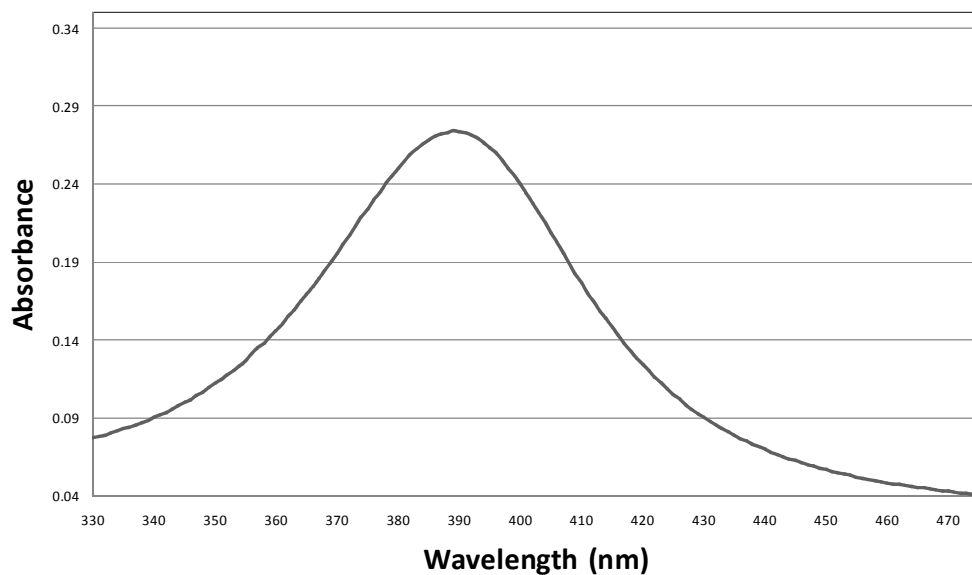


Figure 93. This graph shows the UV vis spectroscopy for the sample M1-26050 in time 1

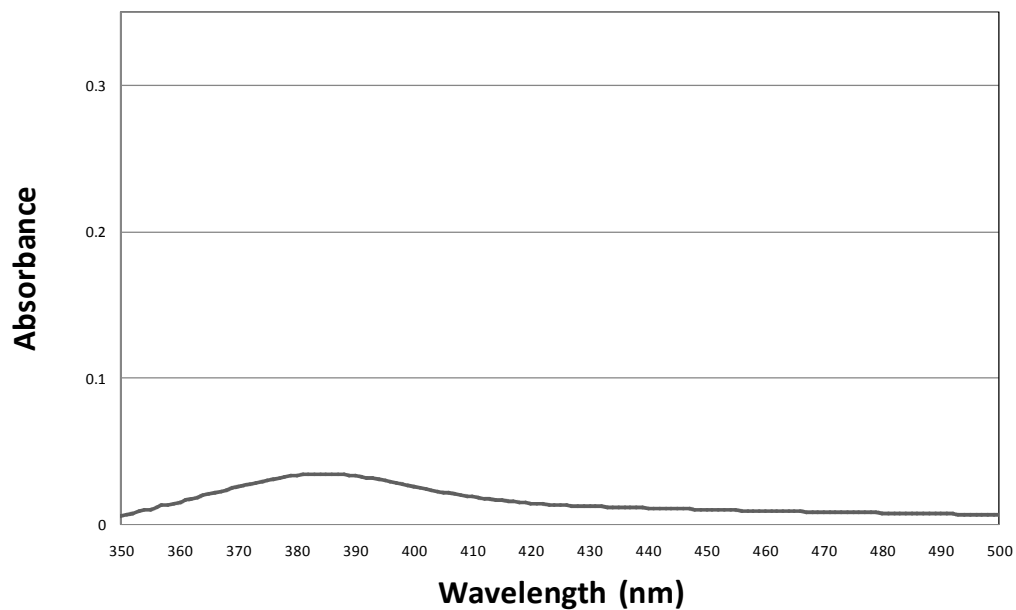


Figure 94. This graph shows the UV vis spectroscopy for the sample M1-26050 in time 2

12 APPENDIX E

Residuals analysis

The residuals values are known as the difference between the response from the experiments and the estimated response from the statistical model obtained from ANOVA analysis. These residuals values need to satisfy the normal distribution, homogeneity on variances and random order in the runs [13]. The following figures from 82 to 93 show the p values for each test of assumptions for residuals. The test was for the analysis of variance and normal probability for *Size 1* and 2 of nanoparticles and the slope, *Z* potential 1 and 2 and the slope. The alpha value (α) used to determine the significance in these tests was 0.05. The test for equal variances generates a plot that displays [Bonferroni 95% confidence intervals](#) for the response standard deviation at each level. Bartlett's and Levene's test results are displayed in the graph. Bartlett's test is interpreted when the data come from normal distributions and Levene's test is used when the data come from continuous, but not necessarily normal distributions, If the p values is larger than 0.05 these data do not provide enough evidence to claim that the populations have equal variances [13].

In the graphical output of plot for normal probabilities versus the data, the data depart from the fitted line most evidently in the extremes, or distribution tails. The Anderson-Darling test's p value indicates that, at a levels greater than 0.05, there is evidence that the data do not follow a normal distribution. That is, these data do not provide enough evidence to claim that the populations have normal distribution [13]. From p values seen in the graphs it is possible to conclude that all assumptions were met for all responses. The Table 7 shows the p values for run order test for all the responses, is easy to see that the responses meets the assumption because the p values were larger than 0.05.

Table 7. Shows the p values for the run order for each response

Run order test (response)	p value	Violation of this assumption?
<i>Size 1</i>	0.078	no
<i>Size 2</i>	0.838	no
<i>Size slope</i>	0.508	no
Z potential 1	0.329	no
Z potential 2	0.850	no
<i>Z potential slope</i>	0.838	no

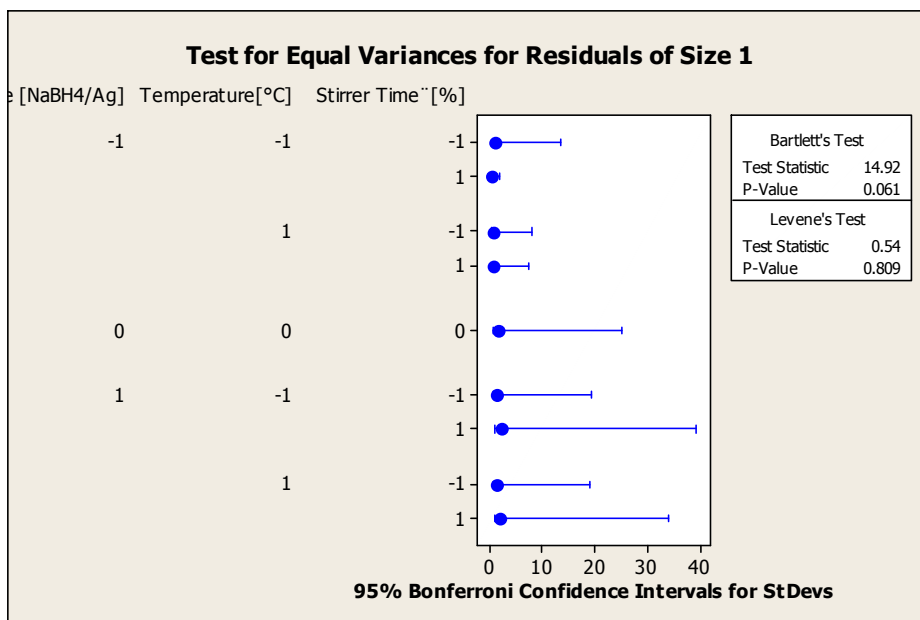


Figure 95. Test for equal variances for residuals of *size 1*

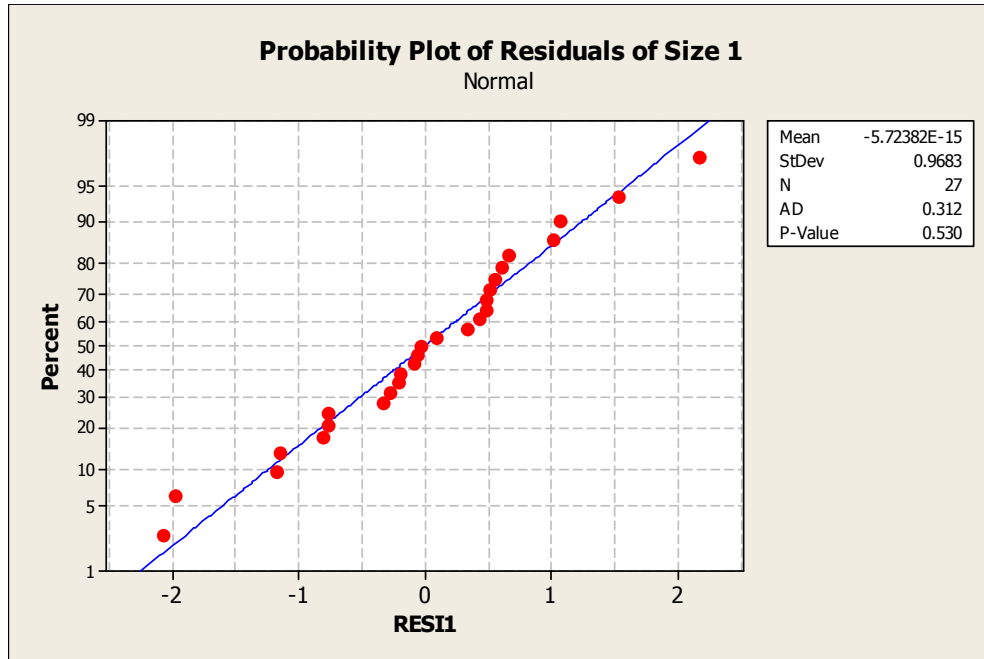


Figure 96. Normality test for residuals of *size 1*

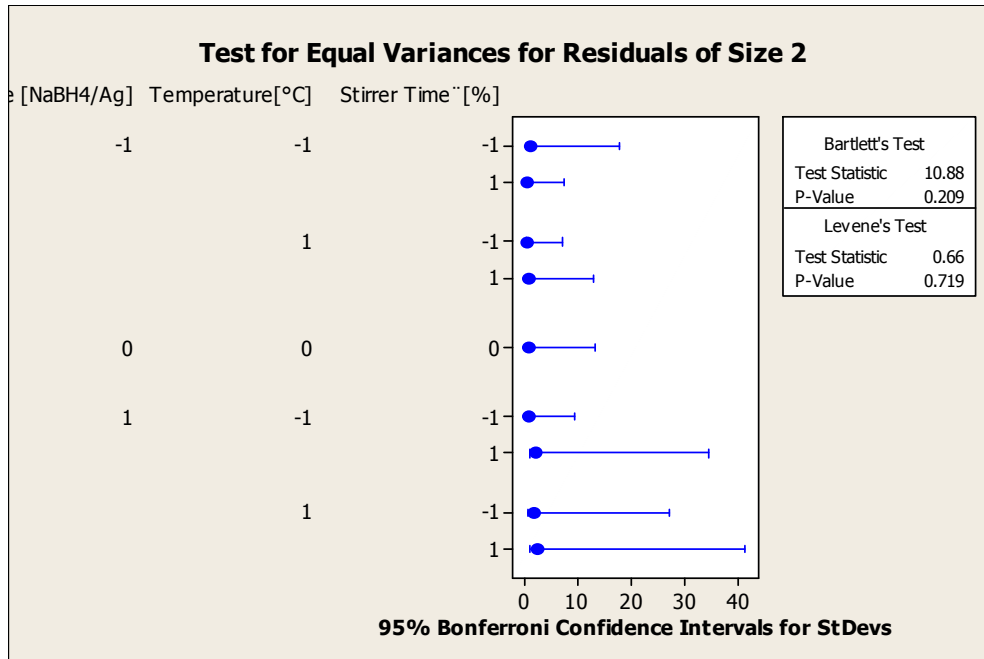


Figure 97. Test for equal variances for residuals of *size 2*

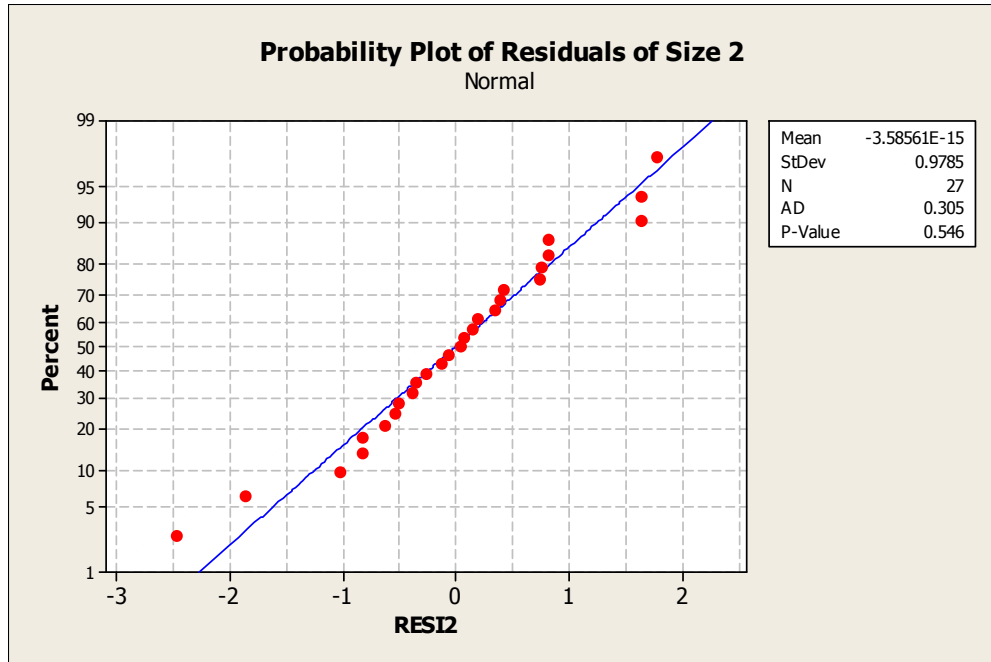


Figure 98. Normality test for residuals of *size 2*

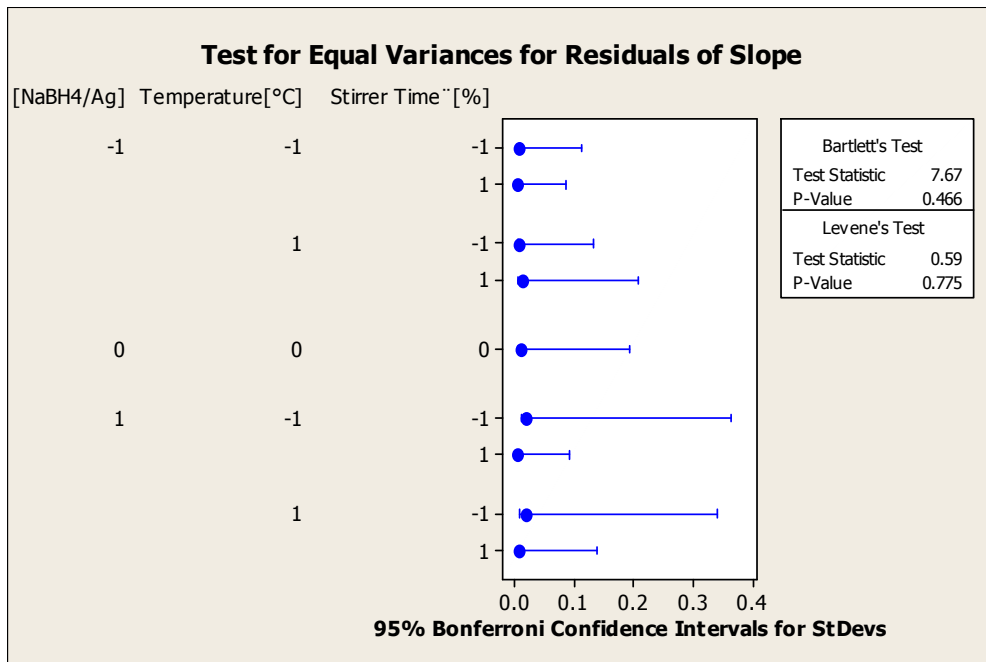


Figure 99. Test for equal variances for residuals of *size slope*

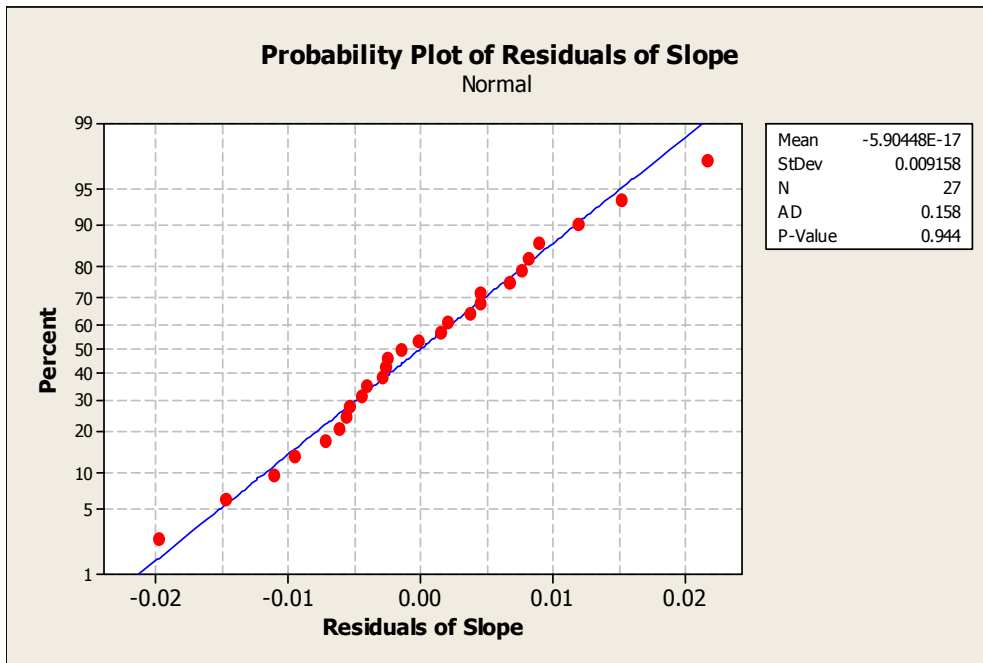


Figure 100. Normality test for residuals of *size slope*

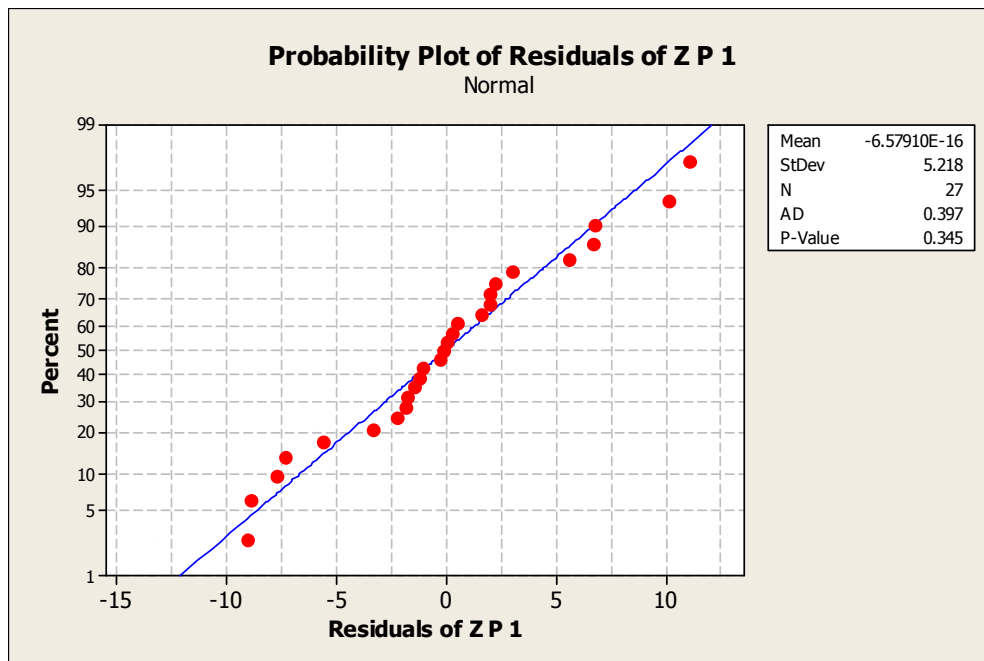


Figure 101. Normality test for residuals of Z potential 1

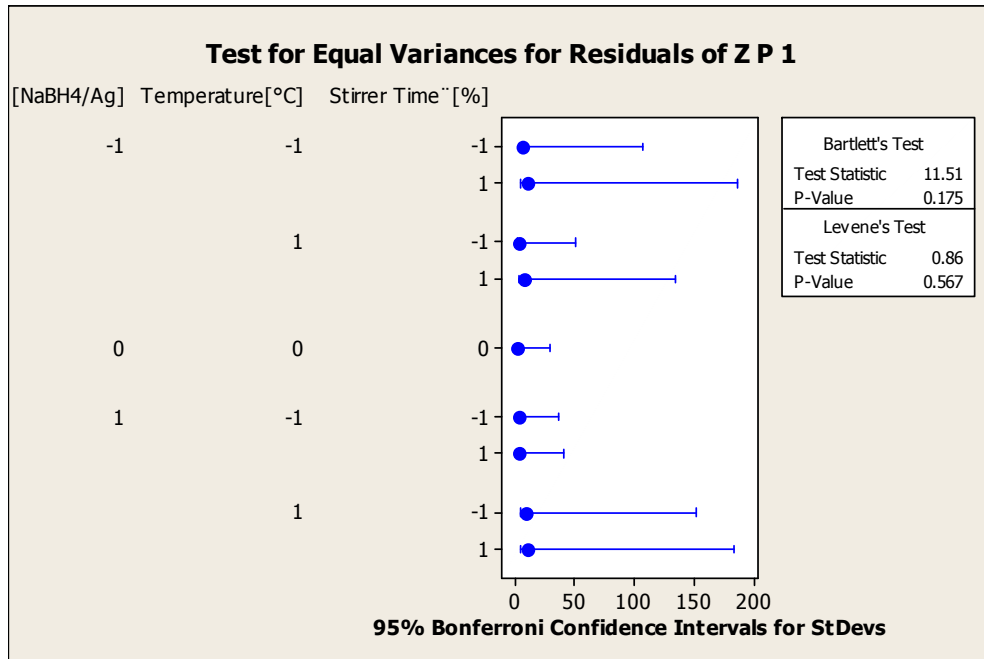


Figure 102. Test for equal variances for residuals of Z potential 1

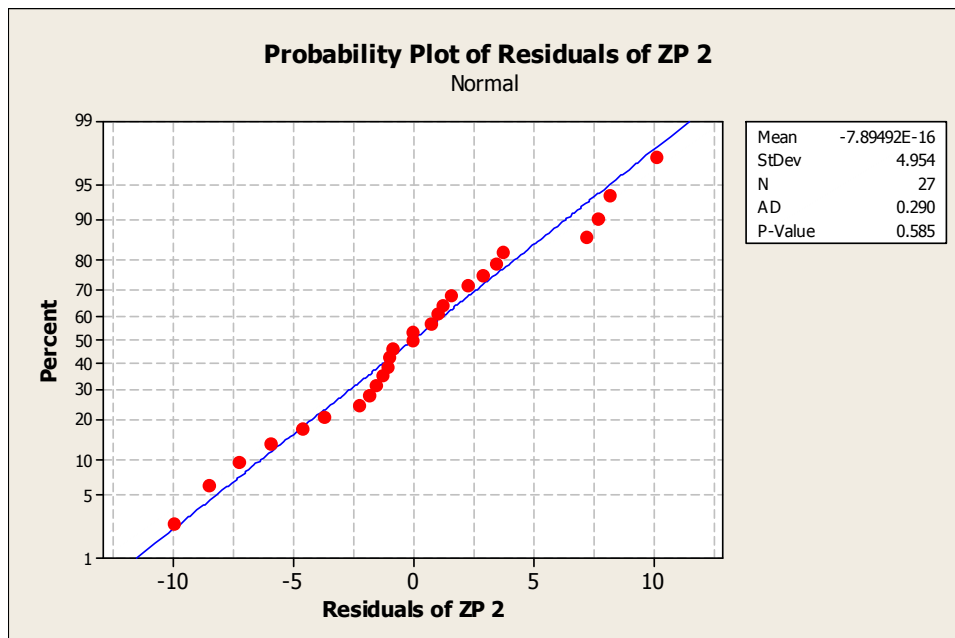


Figure 103. Normality test for residuals of Z potential 2

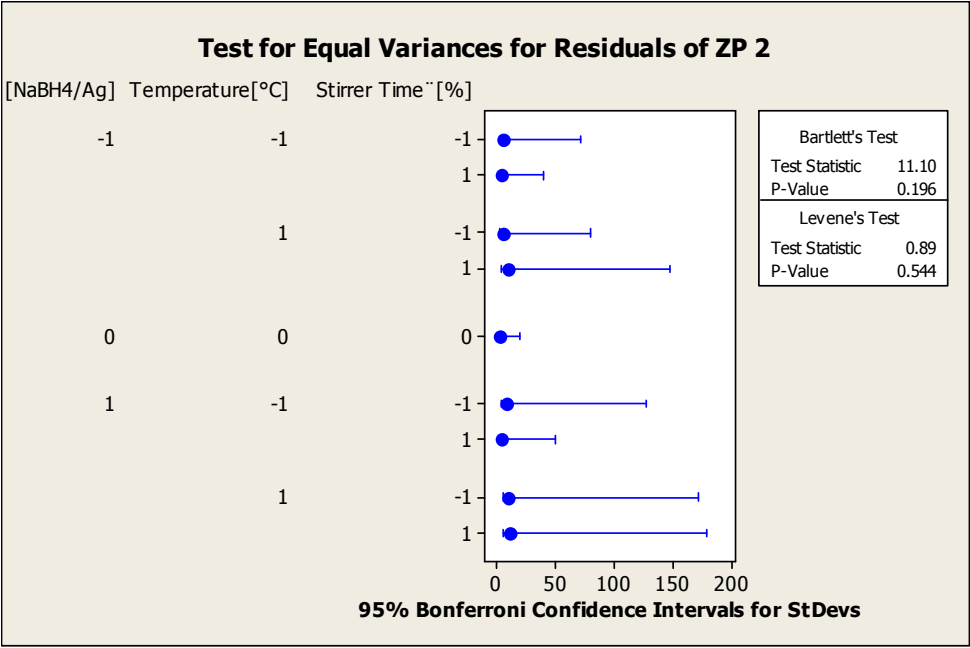


Figure 104. Test for equal variances for residuals of Z potential 2

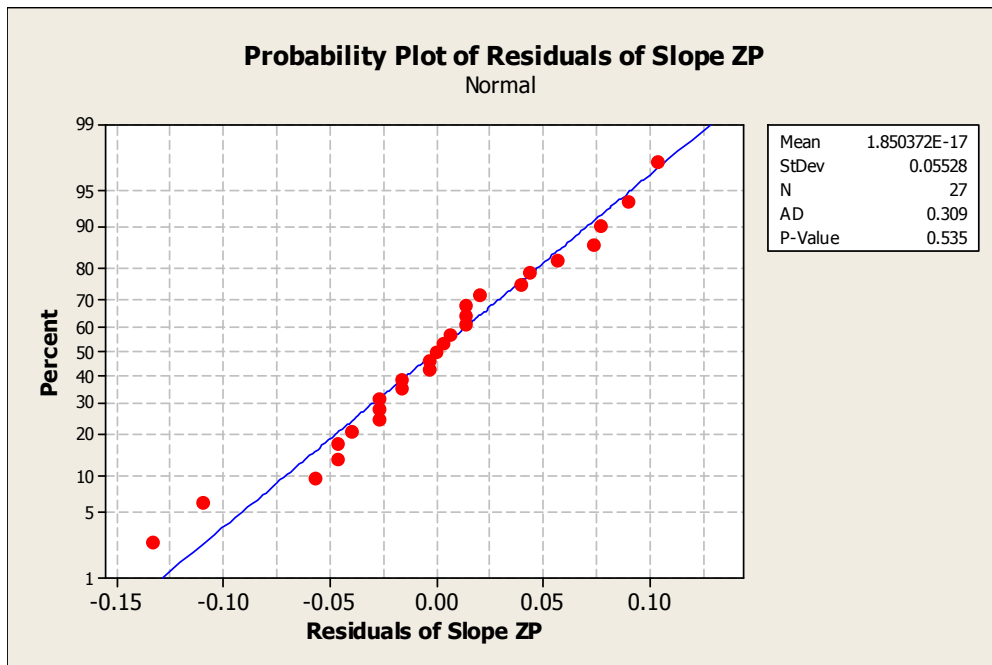


Figure 105. Normality test for residuals of *z potential slope*

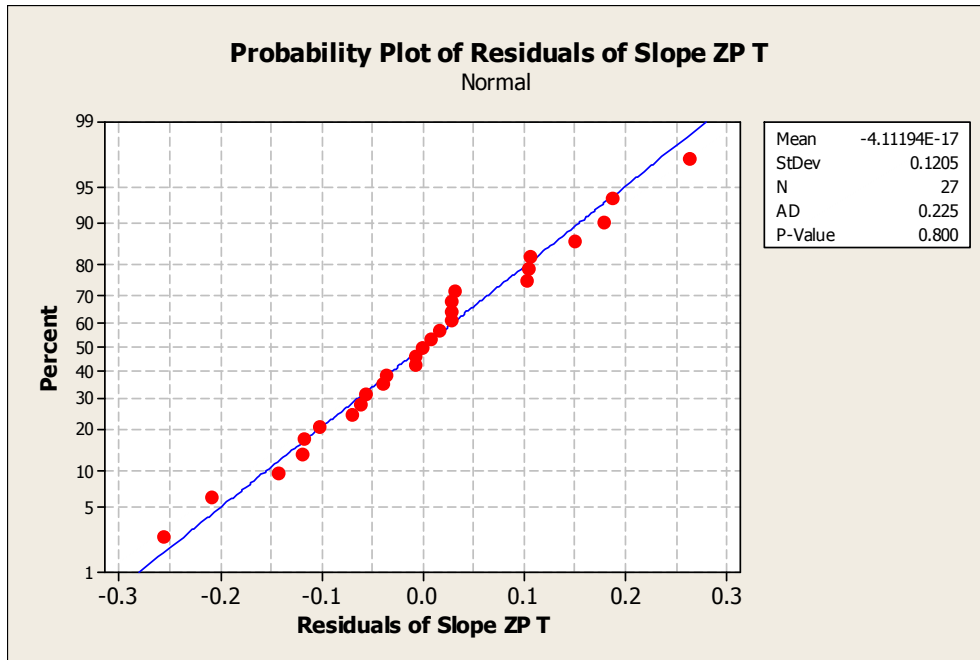


Figure 106. Normality test for residuals of *z potential slope*